Polar oxide surfaces

2000 J. Phys.: Condens. Matter 12 R367

(http://iopscience.iop.org/0953-8984/12/31/201)

J. Phys.: Condens. Matter **12** (2000) R367–R410. Printed in the UK PII: S0953-8984(00)85226-1

REVIEW ARTICLE

Polar oxide surfaces

Claudine Noguera

Laboratoire de Physique des Solides, UMR CNRS 8502, Université Paris-Sud, 91405 Orsay, France

E-mail: noguera@lps.u-psud.fr

Received 18 February 2000

Abstract. In the light of recent experimental as well as theoretical studies, we summarize our present understanding of polar oxide surfaces and examine fundamental issues regarding their stability. The focus is on the surface atomic configurations (relaxations, reconstructions, non-stoichiometry, etc) obtained under specific preparation conditions and their associated electronic structure. We discuss several mechanisms at work on polar surfaces, such as relaxation effects, change of covalency in the surface layers, partial filling of surface states, and stoichiometry variations, and try to assess their actual efficiency for cancelling the polarity.

1. Introduction

Oxide surfaces represent a common denominator of several fields of research which include geology, catalysis, electrochemistry, electronics, magnetic recording, and solid-state physics. They are always present, although in a sometimes uncontrolled way, whenever a material is in contact with the ambient atmosphere. As a result, they play a fundamental role in corrosion, friction, lubrication processes, etc.

It has long been recognized, for example in the field of catalysis or adhesion, that the most efficient surfaces for applications are not necessarily the most perfect ones. Powders are currently used in catalysis mainly because they exhibit numerous micro-facets, separated by edges with atoms in low-coordination environments. Perfect cleavage planes have a very low reactivity, while powders may be active catalysts. This is due to characteristic electronic states associated with the 'defects'. On insulating oxides, their energies are usually located in the gap region, above the top of the bulk valence band and below the bottom of the bulk conduction band. This makes the surface oxygens more basic and the surface cations more acid than their bulk counterparts, and enhances the overall reactivity.

Considering another aspect, nano-structured surfaces are more and more used nowadays, as substrates for growing artificial structures with specific conformations. For example, vicinal surfaces, which exhibit arrays of parallel steps, can be used to make quantum wires: the migration of metallic adatoms on the surface after deposition is driven by the presence of the steps, and the atoms gather in linear chains rather than disperse on the surface. Reconstructed surfaces with large unit cells may also drive specific growth modes, favouring for example the formation of size-controlled clusters.

In this context, polar surfaces of compound materials are of prominent interest. Their orientation is such that each repeat unit in the direction perpendicular to the surface bears a non-zero dipole moment. An electrostatic instability results from the presence of this macroscopic

0953-8984/00/310367+44$30.00

dipole, which can only be cancelled by the introduction of compensating charges in the outer planes. This can be achieved either by a deep modification of the surface electronic structure—total or partial filling of surface states, sometimes leading to surface metallization—or by strong changes in the surface stoichiometry—spontaneous desorption of atoms, faceting, large-cell reconstructions due to the ordering of surface vacancies, etc [1].

Polar surfaces of compound semiconductors have been the subject of intensive work in the past [2]. This is mainly due to the fact that the (100) surface of zinc-blende compounds serves as a substrate for the growth of nearly all III–V and II–VI device layers. As a result, it is *the* single most important surface in semiconductor technology. Concepts for the understanding of surface stability and charge compensation in sp_3-bonded materials have been developed and will be referred to in this review. However, more diversity is met in polar oxide surfaces. They present a vast number of crystallographic structures—rock-salt, corundum, spinel, inverse spinel, wurtzite, perovskite, for the simplest ones—which reflect the subtle mixing of ionicity and covalency in the metal–oxygen bonding and the specificities due to the d electrons in transition metal oxides. In addition, mixed-valence compounds, such as magnetite Fe_3O_4, can form when metal atoms with several oxidation states are involved, and playing with experimental parameters, such as temperature and partial oxygen pressure, allows one to stabilize oxides of different stoichiometries. It is clear that these peculiarities demand a generalization, if not a total reconsideration, of some theoretical concepts.

Compared to metal or semiconductor surfaces, the field of oxide surfaces has only developed within the last ten years, due to difficulties in preparing well-controlled single-crystal surfaces and implementing spectroscopic experiments to access the local atomic and electronic structures. This is the well-known charging problem met in ultrahigh-vacuum-(UHV-) based spectroscopies which involve the emission or scattering of charged particles, such as electrons. Most of these difficulties are nowadays overcome, and several syntheses of our knowledge, especially in the field of non-polar surfaces, have appeared [1, 3].

Currently, the controlled fabrication of ultrathin oxide layers is opening additional new perspectives [4]. First, it gives an answer to the charging problem, since it allows the tunnelling of neutralizing electrons or holes from the substrate. More fundamentally, in growing thin films through the deposition of metal atoms and subsequent oxidation, it becomes possible to produce more open or unstable surface orientations—and polar orientations are among these—than by cutting a single crystal. One can also synthesize metastable phases, or substrate-stabilized phases, in parts of the bulk phase diagram where they would be thermodynamically unstable.

It is the goal of this review to examine fundamental issues regarding polar oxide surfaces, especially in the light of recent experimental as well as theoretical developments. Section 2 summarizes the basic electrostatic concepts underlying the surface instability, the assignment of a surface to the family of polar surfaces, and the condition for cancelling the polarity. Section 3 reviews our present knowledge on specific polar surfaces belonging to various crystallographic classes—rock-salt, inverse spinel, corundum, wurtzite, perovskite structures—with special emphasis on the compounds most thoroughly studied. The discussion, which is the subject of section 4, involves several facets. It first includes a summary of existing analytical models of electronic structure that can support arguments regarding polarity; among these are the ionic model, the electron-counting model, and the bond-transfer model, recently developed in this field, and used for understanding charge distributions in clusters and at surfaces. The latter model is then used to discuss several mechanisms at work on polar surfaces and demonstrate their actual efficiency in cancelling the polarity. Surface relaxation effects, change of covalency in the surface layers, partial filling of surface states, and stoichiometry variations will be considered in this context. Finally, we will conclude with open questions for future investigations.

2. Criterion for surface polarity

2.1. Diverging electrostatic surface energy

According to classical electrostatic criteria, the stability of a compound surface depends on the characteristics of the charge distribution in the structural unit which repeats itself in the direction perpendicular to the surface, as schematized in figure 1 [5]. Type 1 or 2 surfaces—which differ in the charge Q borne by their layers—have a zero dipole moment $\vec{\mu}$ in their repeat unit and are thus potentially stable. In contrast, polar type 3 surfaces have a diverging electrostatic surface energy [6] due to the presence of a non-zero dipole moment not only on the outer layers (which would not distinguish them from non-polar rumpled or reconstructed surfaces), but also on *all* the repeat units throughout the material.

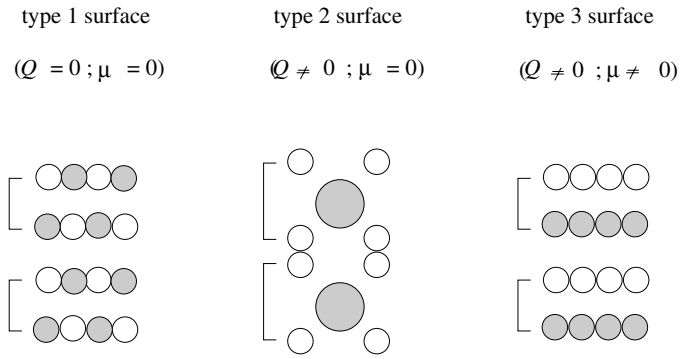

Figure 1. Classification of insulating surfaces according to Tasker [5]. Q and $\vec{\mu}$ are the layer charge density and the dipole moment in the repeat unit perpendicular to the surface (indicated by a bracket), respectively.

The simplest representation of a crystalline compound cut along a polar direction is given in figure 2(a). Two inequivalent layers of opposite charge densities equal to $\pm\sigma$ alternate along the normal to the surface, with interlayer spacings R_1 and R_2. Each repeat unit bears a dipole moment density equal to $\mu = \sigma R_1$, and, as a result, the electrostatic potential increases monotonically across the system by an amount $\delta V = 4\pi\sigma R_1$ per double layer. δV is large, typically of the order of several tens of eV in an ionic material like MgO. The total dipole moment $M = N\sigma R_1$ of N bilayers is proportional to the slab thickness, and the electrostatic energy amounts to $E = 2\pi N R_1 \sigma^2$. It is very large, even for thin films. In the limit $N \to \infty$, the electrostatic contribution to the surface energy per unit area diverges. This is the origin of the surface instability.

2.2. Classification of surfaces

The classification of surfaces relies on the characteristics of the polarization in the bulk unit cell, on the surface orientation $\hat{n}$, and on the nature of the crystal termination.

Recently, a generalized definition of the bulk electric polarization $\vec{P}$ of insulating crystals has been given in terms of the centres of charge of the Wannier functions of the occupied bands. Considering a surface of orientation $\hat{n}$, the bound charge density Q_b which accumulates at a surface is given by $Q_b = \vec{P} \cdot \hat{n}$. It is defined modulo e/A, with A the surface cell area. If $Q_b = 0$ (modulo e/A), the surface is non-polar; otherwise it is polar [7]. $\vec{P}$ can be estimated from the knowledge of the ground-state electronic distribution in the bulk unit cell, which is

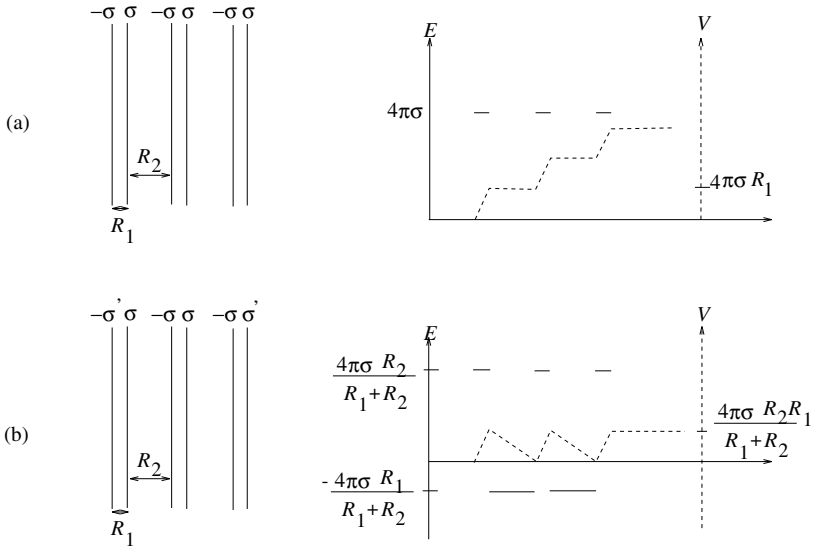

Figure 2. Spatial variations of the electrostatic field E and potential V in a slab cut along a polar direction.

quite accurately provided either by high-resolution x-ray diffraction experiments, as recently shown e.g. for alumino-silicate compounds [8], or by first-principles methods, such as those which are based on the density functional theory (DFT) [9].

Actually, in most cases, simple models for the electronic structure may easily indicate whether a surface is polar or not. In binary compounds, for example, the difference in electronegativity of the constituents readily points to the sign of the charge transfer between the ions. Thus, for simple crystal structures and for orientations such that layers containing cations only and anions only alternate—(100) and (111) zinc-blende surfaces; (111) rock-salt surfaces (see section 3.2); etc—the presence of a dipole moment in the repeat unit is unquestionable, whatever the charge values—provided they are non-zero. These surfaces are undoubtedly polar surfaces. The same is also true for some surfaces of ternary compounds, such as the (110) and (111) faces of ABO_3 perovskites (see section 3.6.2). In $SrTiO_3$, for example, the (110) and (111) repeat units contain alternating SrTiO and O_2 layers in the first case, and alternating SrO_3 and Ti layers in the second one, which are undoubtedly charged, because, in each case, one of the layers in the repeat unit contains a single constituent.

There are less obvious cases, among which is the (100) perovskite surface (see section 3.6.1). In $SrTiO_3$, it presents alternating layers of SrO and TiO_2 composition. If formal charges are assigned to the ions (Sr^{2+}, Ti^{4+}, and O^{2-}), then each layer is charge neutral, the repeat unit bears no dipole moment, and the orientation is considered as non-polar. This is the assertion most often encountered in the literature. However, $SrTiO_3$ is not fully ionic. Its gap width, equal to 3 eV, places it on the borderline between semiconductors and insulators, and the Ti–O bond presents a non-negligible part of covalent character. The actual charges are thus probably not equal to the formal ones and there is little chance that $Q_{Sr} + Q_O$ and $Q_{Ti} + 2Q_O$ vanish. $SrTiO_3$(100) should thus be considered as a polar surface, and this demonstrates how careful one should be in the classification of surfaces.

In addition, the orientation $\hat{n}$ is not always sufficient to characterize a surface, especially when various terminations may be produced. In the rutile structure, for example, in which some transition metal MO_2 oxides crystallize, the bulk repeat unit in the (110) direction is made

of three layers of O and $(MO)_2$ composition, and there exist three chemically inequivalent terminations, which expose a single oxygen layer (O/$(MO)_2$/O sequence), two oxygen layers (O/O/$(MO)_2$ sequence), or one mixed cation–oxygen layer ($(MO)_2$/O/O sequence). Only in the first case does the repeat unit bear no dipole moment. Similarly, on the basal (0001) face of the corundum structure, met in some M_2O_3 sesquioxides (see section 3.4), three chemically distinct terminations may be produced, with a single cation layer, two cation layers, or one oxygen layer in contact with vacuum. Only the first one is non-polar and this is met under standard preparation conditions. However, when experimental conditions are varied—for example, in the process of fabrication of ultrathin films, or under bombardment, or reducing or oxidizing conditions—some variations of stoichiometry in the surface layers may take place and polarity arguments have to be re-examined. The M_2O_3(0001) surfaces are usually discussed in this context and that is why we include them in the present review.

2.3. Electrostatic condition for cancelling the polarity

According to classical electrostatics, ideal polar surfaces are thus unstable. However, specific modifications of the charge density in the outer layers may cancel out the macroscopic component of the dipole moment and cancel the polarity. Within the geometry displayed in figure 2(b), this can be achieved, for example, by assigning a value $\sigma' = \sigma R_2/(R_1 + R_2)$ to the charge density on the outer layers of the slab, and this results in a total dipole moment $M = \sigma R_1 R_2/(R_1 + R_2)$ which is no longer proportional to the slab thickness. The monotonic increase of the electrostatic potential is also suppressed. More generally, when m outer layers are modified ($|\sigma_j| \neq \sigma$ for $1 \leqslant j \leqslant m$ and $|\sigma_{m+1}| = \sigma$), the condition for the cancellation of the macroscopic dipole moment reads [10]

$$\sum_{j=1}^{m} \sigma_j = -\frac{\sigma_{m+1}}{2}\left[(-1)^m - \frac{R_2 - R_1}{R_2 + R_1}\right]. \tag{2.1}$$

A polar surface can thus be stabilized provided that the charge compensation dictated by equation (2.1) is fulfilled. This implies that either the charges or the stoichiometry in the surface layers are modified with respect to the bulk, and thus, several scenarios are conceivable that would cancel the polarity:

- One or several surface layers have compositions which differ from the bulk stoichiometry. This may lead to a phenomenon of reconstruction or terracing depending upon how the vacancies or adatoms order. However, if no ordering takes place, surface diffraction patterns exhibit a (1×1) symmetry and, unless quantitative analysis is performed, give no information on the surface stoichiometry.
- Foreign atoms or ions, coming from the residual atmosphere in the experimental set-up, provide the charge compensation.
- On stoichiometric surfaces, charge compensation may result from an electron redistribution in response to the polar electrostatic field. This is well exemplified in *self-consistent* electronic structure calculations.

Which process actually takes place depends firstly upon energetic considerations. As will become clear in the following, if stoichiometric ideal polar surfaces are not observed, this is never because their surface energy diverges. There always exist enough electronic degrees of freedom in a material to reach charge compensation through the third mechanism. However, in most cases, the resulting surface energy is high and other processes may be more efficient. If experiments are performed in thermodynamic equilibrium conditions, the observed surface configuration is that with the lowest relevant thermodynamical potential (e.g. the grand

potential if the surface is in contact with a reservoir—an oxygen-rich atmosphere, for example). If thermodynamic equilibrium is not reached, the observed surface configuration is that of lowest energy, which is *kinetically* accessible [11].

3. Experimental and theoretical results on polar oxide surfaces

An abundant literature is devoted to the production of polar single-crystal surfaces, the fabrication of thin oxide layers oriented in a polar direction, their atomic and electronic structure depending upon the specific preparation conditions, and finally their reactivity to molecular or metallic adsorption. In the following, we will only discuss those works which refer explicitly to atomic, electronic, or energetic characteristics akin to polarity. The presentation is given according to the crystal structures and the surface orientations. Beforehand, we make some general comments on experimental as well as theoretical requirements for treating polar surfaces.

3.1. Technical comments

Most of the usual techniques of surface science have been applied to investigate the atomic and electronic structure of polar surfaces of insulating materials. However, due to the development of oxide surface science being only recent and due to the difficulty in producing well-characterized and reproducible surfaces, a complete characterization of the surface structure and stoichiometry, which is of such prominent importance, especially in the present field, is lacking for most of the systems which have been considered so far. Despite important advances, it remains a challenge to make quantitative LEED (low-energy electron diffraction) analyses. But the recent development of GIXD (grazing-incidence x-ray diffraction) experiments has yielded a better understanding of non-polar surfaces and has also produced a few results on polar surfaces [12].

Another route to overcoming charging effects, as well as to better controlling heating or cooling processes, consists in producing ultrathin oxide films on conducting substrates [4]. Direct oxidation of a metal single crystal (e.g. Ni to produce NiO) or of an alloy surface (e.g. NiAl to produce Al_2O_3) may be performed, the latter process sometimes yielding a better interfacial coherency when the oxide and its metal have a large lattice misfit. Deposition of metallic atoms on an inert substrate in an oxygen atmosphere, or deposition followed by oxidation—with an oxygen plasma source or other oxidizing agents (e.g. NO_2)—have also been used to produce good-quality oxide films.

On the theoretical side, the simulation of polar surfaces requires special attention. First, as already mentioned, in order to describe accurately the charge distribution in the outer layers, only *self-consistent* electronic structure calculations, which account for the electron density and the electrostatic potential on the same footing, can yield reliable results. In the following we will not mention non-self-consistent or non-*fully* self-consistent calculations which lead to erroneous results. In addition, cluster models for the representation of a polar surface, even if they are embedded in an array of charges or pseudopotentials, are easily biased by finite-size effects, especially when the quantum part of the cluster is small. Most of the recent numerical works make use of slab models. The slabs have to be thick enough to display bulk characteristics in their central layers. When a plane-wave basis set is used for the development of the eigenstates, the slab is repeated in the direction perpendicular to the surface. In order to get rid of spurious interactions between the images, the vacuum region has to be thick enough and the slabs should be symmetric with a zero total dipole moment. However, this is not always possible, for example along the (0001) orientation of wurtzite because of its ABAB sequence.

Several schemes have been proposed in such cases. In one of them, two equivalent slabs, with one the mirror image of the other, are put in contact and fractional charges are introduced in the central layers in order to prevent charge transfer and bonding between like atoms [13]. Another solution consists in saturating the surfaces with fractionally charged hydrogen pseudo-atoms, with a suitably fixed chemical potential [14, 15]. In the case of III–V compounds, introducing a central layer of an element belonging to the IVth column of the periodic table has also been tried [16]. This point should not be considered as satisfactorily solved in the general case.

3.2. The (111) surface of rock-salt oxides

The rock-salt structure consists of two interpenetrating fcc lattices of anions and cations. This structure is one of the most stable ones for highly ionic solids [17]. It is met in alkaline-earth oxides (MgO, CaO, SrO, BaO) and in some transition metal oxides such as NiO, CoO, FeO, TiO, and VO, with cations in a +2 oxidation state. Some of the latter are however very often non-stoichiometric in the cation and/or anion sublattices. The polar orientation of lowest indices is (111). The two-dimensional unit cell is hexagonal and the surface atoms are threefold coordinated. A crystal cut along (111) presents alternating layers of metal and oxygen composition, which are equidistant ($R_2 = R_1$). In an ionic picture, the two-dimensional unit cell bears a charge ± 2, so a reduction of charge by a factor of 2 is required in the outer layers, according to equation (2.1). When charge compensation is provided by changes in stoichiometry, simple electrostatic arguments suggest two stable surface configurations. One is obtained by removing every other atom in the outermost layer, which yields a missing-row surface structure with a (2×1) reconstructed unit cell. This configuration may be thought of as a stacking of non-dipolar M/2O/M repeat units, with zero inter-unit distance. The second stable surface configuration, called the octopolar (2×2) reconstruction [18], is obtained by removing 75% of the atoms in the outermost layer and 25% in the layer beneath, in a way which produces {100} nano-facets. Top views of the unreconstructed, (2×1), and (2×2) surfaces are shown in figure 3.

3.2.1. NiO(111). Single-crystal NiO(111) surfaces [19, 20] as well as thin NiO(111) films grown on various substrates such as Ni(100) [21], Ni(111) [22, 23], and Au(111) [24, 25] have been studied. No reconstruction was found for NiO(111)/Ni(100) [21]. Dynamical LEED analysis has suggested that the terminal layer is made of oxygen atoms and is strongly relaxed inwards (14.8%). All other NiO(111) surfaces considered present p(2×2) LEED patterns, usually attributed to the octopolar reconstruction, whether the films are grown by oxidation of a Ni(111) surface or on Au(111). The lattice mismatch between NiO(111) and Au(111) is smaller than with Ni(111), and the films are of better quality. STM (scanning tunnelling microscopy) experiments furthermore suggested that the surface is terminated by a single type of atoms, due to the presence of steps of a single unit height [24, 25].

GIXD experiments have been performed on single-crystal NiO(111) samples [19, 20]. For air-annealed samples, the structural refinement indicates that the p(2×2) surface is terminated by Ni atoms, as predicted by molecular dynamics simulations of the surface [26]. In contrast, as shown recently [27], both metastable O and thermodynamically stable Ni terminations may coexist, separated by single steps, on NiO(111)/Au(111) films 5 ML (monolayers) thick. After *in situ* annealing and oxidation, however, the p(2×2) single-crystal surface is better described as that of a hypothetical Ni_3O_4 inverse spinel structure.

The p(2×2) surface reconstruction of NiO(111)/Ni(111) disappears in the presence of water [22]. This effect was attributed to the stabilizing presence of hydroxyl groups adsorbed on the outer layers, which provides exact charge compensation. A reversible transition

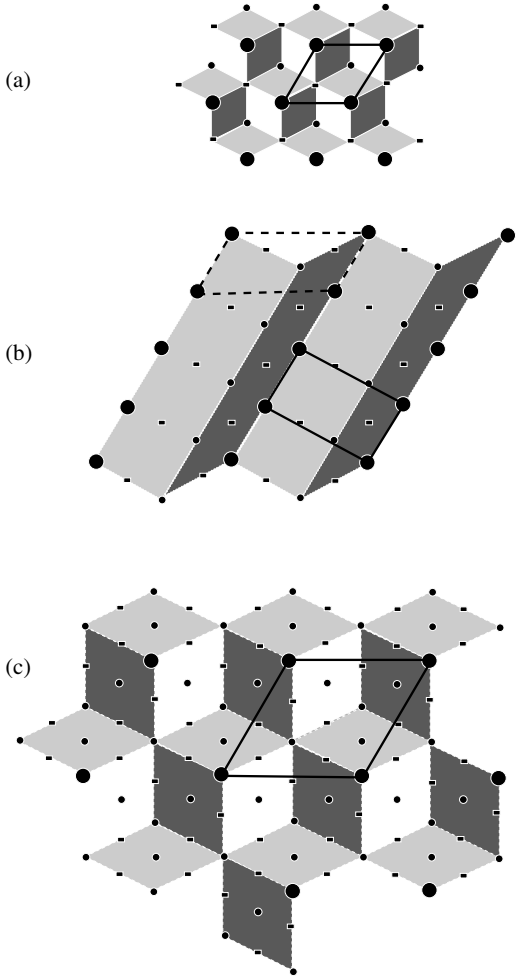

Figure 3. Top views of three surface configurations of a rock-salt (111) surface: (a) the stoichiometric unreconstructed surface; (b) a (2×1) reconstruction obtained by removing every other atom in the top layer; (c) the (2×2) octopolar reconstruction.

between the reconstructed and the non-reconstructed surfaces was evidenced [23]. These results supported the idea that the polar orientation of NiO is more reactive than the (001) cleavage face [4]. However, on NiO(111)/Au(111) surfaces, no deconstruction takes place when the film is exposed to a water-containing atmosphere. Recent attempts to decompose water on single-crystal NiO(111) also failed and suggest that water decomposition only takes place on defective surfaces [27].

NiO(111) has served as a substrate for metal deposition. A good-quality epitaxial Co film was obtained after deposition at high temperature [28], despite the existence of a large lattice mismatch between Co and NiO (18%). GIXD experiments evidenced a deconstruction of the substrate, a fact attributed to the metallization of the NiO surface by Co. Similarly, growth of single-crystal $Ni_{80}Fe_{20}$ films was achieved after annealing, but the thermal treatment induces a diffusion of Fe atoms into the substrate and the formation of an interfacial compound of spinel structure of the $FeNi_2O_4$ type [29].

3.2.2. MgO(111). Early attempts to produce (111) surfaces by truncation of bulk MgO led to non-planar surfaces exposing micron-sized triangular facets, as evidenced by LEED and scanning electron microscopy experiments [30, 31]. They were interpreted as {001} facets, the most stable in the rock-salt structure, but recently Plass *et al* [32] have argued that they are actually {111} facets resulting from acid etching in the sample preparation.

Three air-stable reconstructions have been observed by transmission electron microscopy, on MgO(111) samples annealed above 1450 °C [33], namely $(\sqrt{3} \times \sqrt{3})$R30°, (2×2), and $(2\sqrt{3} \times 2\sqrt{3})$R30°. A structure refinement suggests that, for all of them, building units in the surface layers are made of oxygen trimers centred over underlying Mg atoms, as represented in figure 4. This interpretation is in conflict with the (2×2) octopolar model, and none of the surface configurations—assumed to be stoichiometric—proposed in reference [33] fulfils the electrostatic condition (2.1). Further work is required to assess the reconstructed structures.

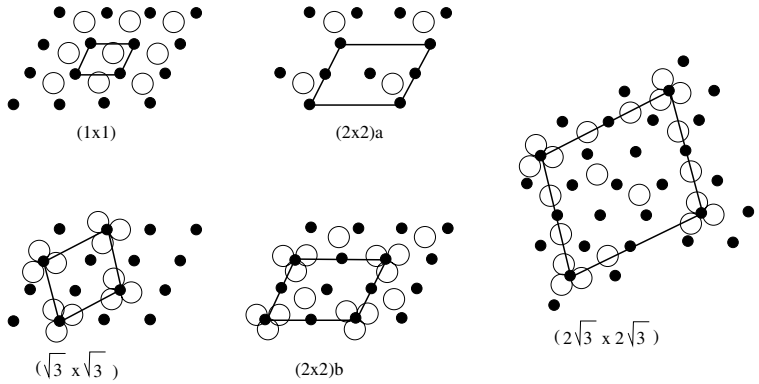

Figure 4. Top views of the $(\sqrt{3} \times \sqrt{3})$R30°, (2×2)b, and $(2\sqrt{3} \times 2\sqrt{3})$R30° reconstruction models of MgO(111), according to reference [33]. The surface is oxygen terminated and the two outermost layers are represented. Black and white circles are the magnesium and oxygen atoms, respectively. The unreconstructed (1×1) and the octopolar (2×2)a surface configurations are also shown for reference.

Good-quality planar surfaces are more easily obtained when a thin oxide film is grown on a substrate. This was the case for MgO(111) layers grown on mica [34] which showed an enrichment in magnesium.

Several quantum mechanical studies of the unreconstructed MgO(111) surfaces have been performed, using a DV-X_α method (DV $\equiv$ discrete variational) on a cluster model [35], a semi-empirical Hartree–Fock method in a slab geometry [36], or a DFT–GGA approach (generalized gradient approximation), also in a slab geometry [37]. All of them evidence a metallicity of the outer layers, arising from important shifts and overlap of the surface valence and conduction bands, as exemplified in figure 5. This produces a large reduction of charge in the surface layers, which fulfils the electrostatic criterion. At variance with ionic models, the calculated surface energy is large ($E_s > 5$ J m^{-2}), but not diverging. This however suggests that the unreconstructed surface is not the lowest-energy configuration. Indeed, in the simulation of stoichiometric surfaces with larger unit cells, a spontaneous desorption of half of the surface atoms takes place in the process of geometry optimization [36].

Simulations of reconstructed surface structures have been performed either using classical pair potential methods [38–41], or with total-energy calculations based on quantum mechanical approaches [36]. They have considered the (2×1), the octopolar (2×2), and the micro-faceted $(\sqrt{3} \times \sqrt{3})$R30° and $(2\sqrt{3} \times 2\sqrt{3})$R30° surfaces. The (2×2) surface energy is found to be

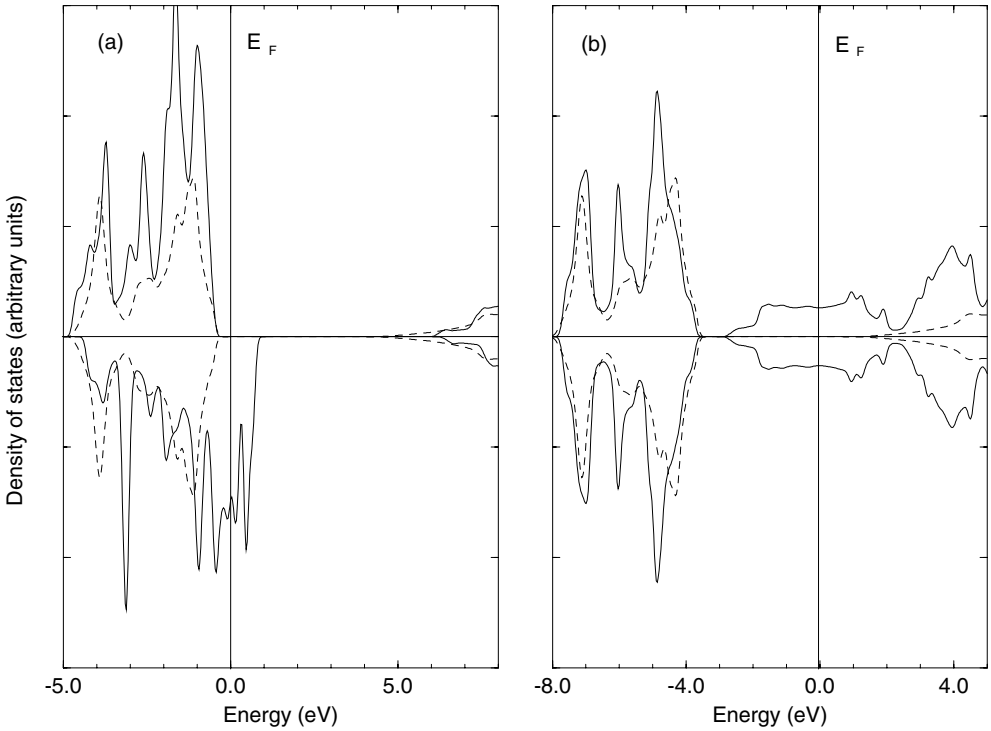

Figure 5. Calculated DOS for five-layer symmetric MgO slabs, with oxygen (a) and magnesium (b) terminations. Plain and dashed lines represent the DOS in the slab and in the bulk, respectively. The top and lower panels refer to projections on majority- and minority-spin states, respectively. All DOS have been convoluted with a 0.1 eV wide Gaussian function (from reference [37]).

lower than the (2×1) one. However, due to the lack of a grand potential calculation, one cannot tell in which range of oxygen partial pressure each surface termination is thermodynamically stable.

The relative stability of hydroxylated MgO(111) and (100) surfaces has been studied in order to explain the frequent occurrence of (111) orientations in the natural growth faces of periclase (the mineral name of MgO). The formation of hydroxyl groups on the two (111) terminations provides the compensating charges required for surface stabilization, and the hydroxylated (111) face is found to be more stable than the (100) one [36, 42]. As a first step towards the simulation of oxide dissolution in water under acidic conditions, the replacement of Mg^{2+} ions by protons on a nano-faceted MgO(111) surface in contact with water has been modelled, using classical simulations [41]. Dissolution appears to be energetically more favoured on sites of lower coordination number.

Various metals have been deposited on MgO(111), for example Cu [43], bcc transition metals [44], Pd [45], and Ni [46]. The substrates were not always well characterized, as in the case of references [44, 45]. In reference [46], the substrate is smooth, non-faceted, and unreconstructed, but probably hydroxylated. On freshly cleaved MgO(111) surfaces, exhibiting no superstructure, but probably {100} facets, copper atoms bind to three oxygens, at a missing-magnesium lattice position, in the first stages of nucleation [43].

There is recent experimental evidence of structurally [47–50] abrupt Cu/MgO(111) and Pd/MgO(111) interfaces produced by internal oxidation of CuMg or PgMg alloys. In the case

of Cu/MgO, the MgO crystallites exhibit (100) and (111) facets whose ratio is a function of the partial oxygen pressure p_{O_2} in the apparatus. The nature of the Cu/MgO(111) interfacial bonds changes from Mg–Cu to O–Cu as p_{O_2} increases [51, 52]. According to *ab initio* calculations performed on the Cu/MgO(111) interface, the adhesion of copper is greatly enhanced on the (111) face, with respect to the (100) one [53, 54], and interfacial electronic states of the metal-induced gap states type are strongly localized at the Cu/O–(111) contact. They have been observed by EELS (electron energy-loss spectroscopy) [55]. The adsorption of a palladium monolayer on MgO(111) and (100) presents similar trends and the stabilizing effect of metal adsorption for cancelling the polarity has been discussed [37].

3.2.3. CoO(111). Thin cobalt oxide films were obtained through oxygen chemisorption on Co(0001) and heating. Epitaxial CoO(111) layers are first produced, but beyond some critical temperature and at high oxygen exposures, Co_3O_4(111) layers are formed [56]. The same sequence occurs when a Pt alloy containing about 20 at.% of cobalt is oxidized [57].

Ultrathin CoO(111) films have been recently synthesized either by oxidation of Co(0001) [58–60] or by deposition and oxidation of metallic atoms on Au(111) substrates [61]. The CoO surface displays a (1×1) LEED diagram, probably due to the presence of hydroxyl groups. Attempts to remove them without damaging the film were unsuccessful. The combined use of HREELS (high-resolution EELS) and NEXAFS (near-edge x-ray absorption fine structure) to probe NO adsorption on CoO(111) [60] has suggested that the surface is metal terminated, in contrast to NiO(111) which can have O-terminated terraces, a difference tentatively attributed to the larger degree of covalent character of the metal–oxygen bond in CoO.

As revealed by GIXD experiments, the (111) surface of a CoO single crystal is covered with an epitaxial Co_3O_4(111) layer of spinel structure, with the epitaxial relationships $Co_3O_4(111) \parallel CoO(111)$ and $Co_3O_4[100] \parallel CoO[100]$. Air annealing of the surface, as well as UHV annealing and Ar^+ bombardment, lead to the creation of metallic Co islands but cannot restore the CoO stoichiometry [62].

3.2.4. FeO(111). Iron oxide films can be formed by different methods, ranging from the direct oxidation of metallic Fe(110) and (111) surfaces [63], to the deposition and oxidation of Fe atoms on Pt(100) and (111) [64–70], Mo(100) [71], Cu(100) [72], or α-Al_2O_3(0001) [73]. Usually FeO, which corresponds to the lowest oxidation state of iron, is produced first, while in the subsequent steps of film growth, other oxides are formed, such as Fe_3O_4 or Fe_2O_3. However, the precise sequence depends upon the substrate, which can influence the iron–oxygen phase diagram at such low thicknesses. In this section, we restrict our consideration to iron monoxide films.

By oxidizing Fe(110) and (111) surfaces [63], FeO(111) films are produced in a (2×2) reconstructed state, in close analogy to NiO(111). Spin-polarized secondary-electron spectroscopy experiments [74] evidence a ferromagnetic order at the surface above the Néel temperature, which was tentatively attributed to the peculiarities of magnetic interactions on an octopolar (2×2) surface. An alternative explanation is the existence of some Fe^{3+} ions at the very surface, as in Fe_3O_4, which is indeed ferrimagnetic.

On Pt(100) and (111) substrates [64–70], FeO films consist of hexagonal close-packed iron–oxygen bilayers that are laterally expanded with respect to bulk FeO and slightly rotated with respect to the Pt substrate. This leads to coincidence structures with large periodicities, e.g. $c(2 \times 10)$ in the case of Pt(100) [68]. On Pt(111) the growth is layer by layer up to two bilayers [70, 75]. Films made of a single bilayer have been the subject of thorough studies [65, 70, 75, 76] by means of STM and XPD (x-ray photoelectron diffraction). The outer layer

is made of oxygen atoms and the interlayer spacing is strongly reduced with respect to that for bulk FeO (0.68 Å versus 1.25 Å). This amounts to a reduction of the Fe–O bond lengths from 2.15 to 1.95 Å. This relaxation is consistent with a quantitative interpretation of STM images [77].

At all thicknesses, the FeO(111) lateral lattice constants are larger than in bulk FeO, and for coverages above 1.5 bilayers, they are even larger in the second layer than in the first one [70, 75]. Such an expansion cannot be attributed straightforwardly to the interaction with the Pt(111) substrate, whose lattice parameter is even smaller than that of FeO (2.77 Å versus 3.04 Å). It is proposed that the driving mechanism is the reduction of the total dipole moment of the film, via a contraction of the interlayer distances, possibly accompanied by a reduction of charge due to an enhancement of covalency. In order to maintain a roughly constant Fe–O bond length, lateral expansion has then to take place.

When iron oxides are grown on an α-Al_2O_3(0001) substrate, usually α-Fe_2O_3(0001) films are obtained. However, in the first stages of growth, a metastable FeO(111) bilayer forms, in which the Fe^{2+} ions are replaced by Fe^{3+} species [73] (figure 6).

The reactivity of FeO(111) films was tested by investigating the adsorption of ethylbenzene [78, 79] and water [80]. In both cases, only weak interactions with the substrate take place. The inertness of the surface was attributed to its oxygen termination, the reactive iron atoms being hidden below the surface layer.

3.2.5. Summary. The polar instability of the rock-salt (111) surface seems to be very strong. There is almost no evidence that an unreconstructed stoichiometric surface exists. This is in agreement with quantum mechanical results, which predict the stoichiometric (1 × 1) configuration (1) to have a very high surface energy, due to its metallic character, and (2) to be not even metastable since a spontaneous desorption of surface atoms takes place when enough structural degrees of freedom are allowed in the simulation. There are nevertheless two reports of unreconstructed surfaces. One concerns NiO(111)/Ni(100) [21] and the other the FeO(111) bilayer grown on Pt. As regards NiO(111)/Ni(100)—a result which has not been reproduced by other authors—it may be that the surface layers were not stoichiometric—in a way which provides charge compensation—but with disordered vacancies. It is likely that dynamical LEED analysis, due to the multiple-scattering treatment of electron diffraction, cannot give quantitative results when both the surface structure and the surface stoichiometry are unknown. The FeO(111) bilayer, on the other hand, does not pertain to the semi-infinite polar surface family. The concept of cancellation of the *macroscopic* dipole moment does not apply to it, due to the presence of only two layers (see section 4.2.5). The observed strong interlayer relaxation is a convincing argument in favour of the lowering of surface energy via dipole reduction.

The observation of octopolar reconstructions on NiO(111) and FeO(111) supports the electrostatic view of cancelling of the polarity. It does not seem very clear at this stage under which experimental conditions the metal or oxygen terminations are thermodynamically favoured. Further work is needed to understand the high-temperature NiO(2×2) reconstruction and the three reconstructions observed on air-annealed MgO.

The stabilizing effect of water and metal adsorption is not fully assessed. The deconstruction of NiO(111) thin films by hydroxylation takes place mainly on defective surfaces. It should however be stressed that the transformation from a (2 × 2) octopolar reconstruction into a (1 × 1) hydroxylated one requires a significant mass transport, probably associated with high activation barriers, making it kinetically limited. A similar question arises when metal adsorption is considered, for example in Co/NiO(111). The internal oxidation of PdMg or CuMg alloys, on the other hand, yielding a precipitation of MgO crystallites, or the

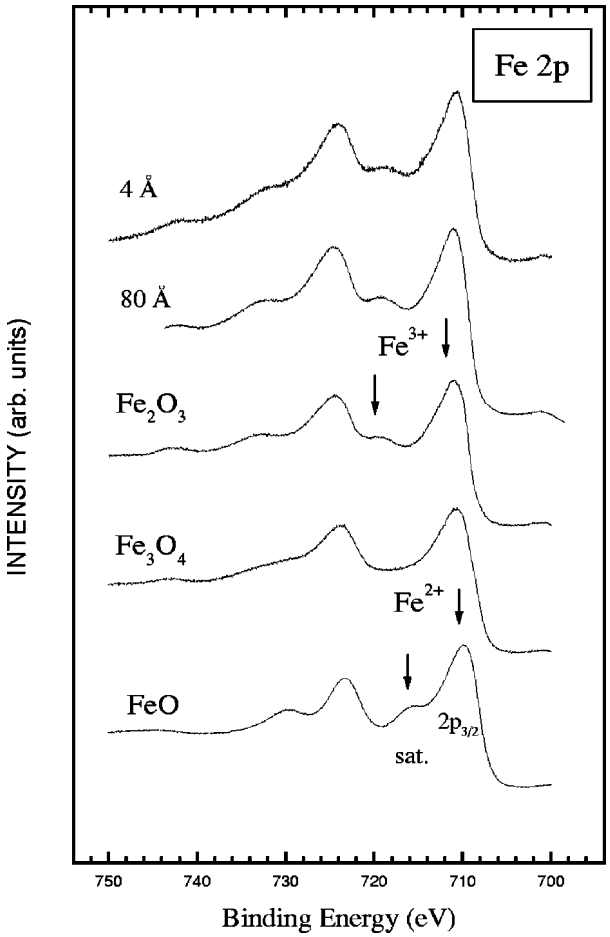

Figure 6. Fe 2p XPS spectra corresponding to iron oxide films of 80 and 4 Å thickness, grown on α-$Al_2O_3(0001)$ at 250 °C. For comparison, three reference spectra of α-Fe_2O_3, Fe_3O_4, and FeO are included. The Fe $2p_{3/2}$ main peak and satellite corresponding to Fe^{3+} and Fe^{2+} are pointed out for α-Fe_2O_3 and FeO, respectively. From reference [73].

growth of MgO faces in a humid atmosphere, are associated with different thermodynamical conditions, which do not require a deconstruction of a pre-established clean surface. However, the electron microscopy studies on the Cu/MgO or Pd/MgO interfaces do not indicate accurately whether the surface is actually planar or nano-faceted.

3.3. Polar (111) and (100) surfaces of inverse spinel compounds

Magnetite Fe_3O_4 crystallizes in the inverse spinel structure. It is based on a slightly distorted face-centred cubic lattice of oxygen atoms, with the iron ions located in the tetrahedral A and octahedral B interstitial sites. Formally, A sites are occupied by ferric ions Fe^{3+}, while B sites contain an equal amount of ferrous Fe^{2+} and ferric Fe^{3+} ions. Above a characteristic temperature known as the Verwey temperature, magnetite possesses a high conductivity which results from electron hopping between the Fe^{2+} and Fe^{3+} species in the B sites. Below this temperature, a drop of conductivity by two orders of magnitude takes place, associated with

a freezing of the hopping processes and accompanied by a structural change from cubic to monoclinic. Fe_3O_4 is a ferrimagnet with a Curie temperature of 858 K.

Magnetite possesses two polar surfaces of low index, the (100) and (111) faces, which are represented in figure 7. The (100) stacking consists of pairs of planes, one containing only tetrahedral Fe^{3+} ions at A sites and the other containing both oxygens and Fe^{2+} and Fe^{3+} ions at octahedral B sites. Surface Fe ions are twofold coordinated. Per unit cell, the layer charge density is formally equal to ± 6, which requires a compensation of charge of ± 3 according to equation (2.1) ($R_1 = R_2$).

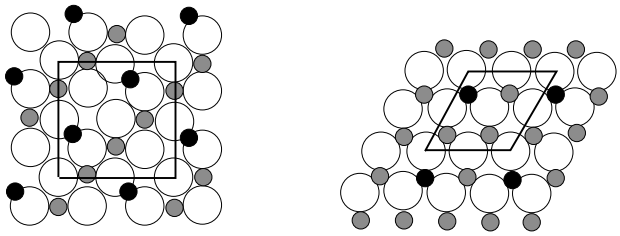

(100) (111)

Figure 7. Top views of the (100) and (111) polar surfaces of magnetite Fe_3O_4. Large open circles are oxygen atoms, small black and grey circles are iron atoms in tetrahedral (A) and octahedral (B) sites, respectively. For the (100) surface, the octahedral irons are in the plane of the oxygens. The (111) stacking represents the $Fe_A/4O/3Fe_B$ sequence with tetrahedral irons on top.

Along the (111) direction, the stacking sequence contains two formula units and is described by $Fe_A/4O/3Fe_B/4O/Fe_A/Fe_B$. Using the bulk interlayer spacings yields a dipole moment in this repeat unit equal to 29.5 D (D $\equiv$ debye). Six different terminations may be produced, each being characterized by its own values for the compensating charges. For the one represented in figure 7, the surface Fe_A ions are threefold coordinated.

3.3.1. Fe_3O_4(100). The (100) surface of magnetite single crystals was thoroughly imaged by STM, at an atomic resolution level, with or without a magnetic tip [81–84]. The use of a magnetic tip allows a discrimination between Fe^{2+} and Fe^{3+} species on the B sites, even above the Verwey transition, and the presence of a Wigner glass, with electron pairs localized on adjacent ions, could be evidenced. The surface state is a function of the preparation conditions: some protrusions—not well resolved—were ascribed to Fe^{3+} ions at A sites, forming 'worm-like' features.

Fe_3O_4(100) thin films on MgO(100), as well as on other cubic substrates, such as $SrTiO_3$(100) or $MgAl_2O_4$(100), have been produced by reactive vapour deposition methods, with the goal of studying their magnetic properties [85–87]. A p(1 $\times$ 1) reconstruction—with respect to the Fe_3O_4 bulk unit cell—was observed. It was attributed to a clustering of atoms in the unit cell, driven by the tetrahedral Fe^{3+} ions [88]. This same reconstruction—elsewhere labelled $(\sqrt{2} \times \sqrt{2})$R45° with reference to the surface unit cell of the unreconstructed surface—was attributed to the ordering of tetrahedral iron vacancies required to achieve charge neutralization [89–91]. The Fe^{3+} /Fe^{2+} ratio as determined by core-level photoemission spectroscopy was higher than in the bulk, and there was no evidence of surface oxygens or hydroxyl groups [91].

More recently, magnetite films have been grown on MgO(100) substrates, using NO_2 as an oxidizing agent. Depending upon the relative fluxes of Fe and NO_2, stoichiometries ranging from Fe_3O_4 to maghemite γ-Fe_2O_3 were obtained [92]. The films grow fully epitaxially in a

layer-by-layer mode. They are (100) oriented with their cubic axes oriented parallel to those of MgO and present a small tetragonal distortion. RHEED (reflection high-energy electron diffraction) and LEED patterns reveal a p(1×1) reconstruction. According to electron-counting arguments, two surface configurations were proposed, corresponding either to a half-filled A layer with one Fe^{3+} ion per unit cell, or to an oxidized B layer with oxygen vacancies or hydroxyl groups [93].

3.3.2. $Fe_3O_4(111)$. The first report of the formation of an ordered magnetite (111) film on Pt(111) was given in references [94, 95]. The magnetite structure was identified by dynamical LEED analysis, and was shown to consist of an unreconstructed (111) termination exposing 1/4 monolayer of Fe over a distorted hexagonal oxygen layer (the $Fe_A/4O$ sequence in the bulk repeat unit). Strong relaxations were found, both for the outermost iron plane ($41 \pm 7\%$) and for the three underlying layers [96]. The stabilization of the termination was attributed to the existence of these large atomic displacements, associated with an enhanced covalency in the surface layers.

XPS and UPS (x-ray and ultra-violet photoemission) experiments as well as XAS (x-ray absorption spectroscopy) [67] showed the structural and chemical identity of the epitaxial films with ones in earlier studies on bulk materials [97]. The shape of the absorption O K edge reveals a hybridization of oxygen states with both Fe 3s and 4s4p orbitals, and is understandable within the framework of ligand-field theory. Angle-resolved photoemission in conjunction with synchrotron radiation gives information on the electronic structure (figure 8) above and below the Verwey transition, and suggests that Fe_3O_4 can be treated by band theory [98]. STM images [99] show surface protrusions which are attributed to the topmost Fe atoms, considering the Fe 3d contribution to the density of states near the Fermi level. The most important point defects are attributed to iron vacancies.

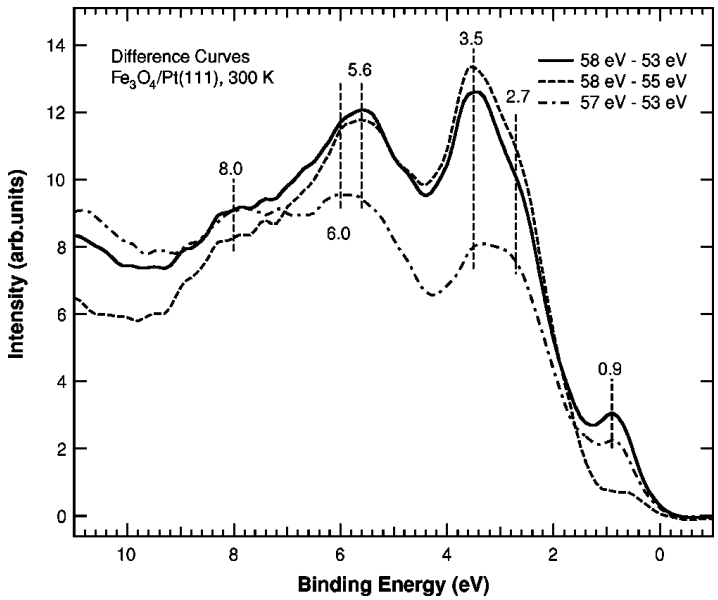

Figure 8. Difference curves for normal-emission spectra taken at 300 K just above and below the Fe 3p $\rightarrow$ 3d resonant photoemission, in Fe_3O_4/Pt(111). Vertical dashed lines indicate the Fe 3d-derived final states involved in the resonance. From reference [98].

On Pt(100) [68], $Fe_3O_4(111)$ thick films have the same surface structure as $Fe_3O_4(111)$ multilayers grown on Pt(111) [69].

An $Fe_3O_4(111)$ epitaxial layer also forms after argon bombardment and annealing in oxygen of an α-$Fe_2O_3(0001)$ (reference [100]) or on an α-$Al_2O_3(0001)$ substrate (reference [101]). Other surface orientations can be produced by choosing suitable substrates (reference [102]). For an α-$Fe_2O_3(0001)$ substrate, the STM images are consistent with a termination by 1/4 ML of Fe [100].

On natural single-crystal $Fe_3O_4(111)$ surfaces prepared in oxygen, two different surface terminations have been imaged by STM [103]: an unreconstructed configuration which exposes 1/4 ML of O atoms over 3/4 ML of Fe, and another unreconstructed termination which exposes 1/2 ML of iron over a close-packed oxygen layer. In more reducing conditions, FeO(111) and $Fe_3O_4(111)$ domains coexist, a phenomenon called biphase ordering.

An *ab initio* Hartree–Fock study in a slab geometry (reference [104]) predicts that the termination by an iron bilayer ($Fe_B/Fe_A/4O/\cdots$ sequence) is energetically favoured, thanks to an exchange of iron and oxygen layers in the slab, which reduces the total dipole moment. It is suggested that the stability of an Fe monolayer-terminated slab ($Fe_A/4O/\cdots$ sequence) may be enhanced by adsorption of hydrogen: the calculated relaxations then agree with the LEED structure refinement performed in reference [95].

At low water coverages, dissociation of H_2O takes place probably at surface iron sites, the neighbouring oxygens acting as proton acceptors [80].

3.3.3. Summary. There have been reports of reconstructions of $Fe_3O_4(111)$ and (100) surfaces, attributed to charge-compensation effects. However, the $Fe_3O_4(111)$ grown on Pt can be obtained unreconstructed. Several effects may be responsible for such an observation: a lack of order of the surface vacancies, the thinness of the layer, or the existence of several oxidation states of iron.

3.4. The corundum (0001) surface

Aluminium oxide as well as transition metal sesquioxides (Cr_2O_3, Ti_2O_3, V_2O_3, Fe_2O_3) crystallize in the corundum structure. Along the (0001) direction, it is composed of hexagonal close-packed oxygen layers with the ABAB$\cdots$ sequence. The oxygen layers alternate with two metal layers, very close to each other, which contain metal atoms in octahedral environments. The bulk unit cell contains 30 atoms (six formula units).

Along (0001), the layer sequence is $M/O_3/M$, with a very short inter-unit distance d (e.g. 0.485 Å in Al_2O_3), as shown in figure 9. As a result, three chemically distinct terminations may be produced, which expose a single metal layer ($M/O_3/M/\cdots$), an oxygen layer ($O_3/M/M/\cdots$), or two metal layers ($M/M/O_3/\cdots$). Only the first repeat unit bears no dipole moment. In this configuration, the surface metal atoms are threefold instead of sixfold coordinated in the bulk. Because the M–M interplane distance d is so short, some authors describe the structure as the result of a piling of M_2 and O_3 layers. They thus consider that (0001) is a polar orientation, which can only be stabilized by non-stoichiometry in the surface layer. By removing half of the surface metal atoms, compensation is indeed achieved, with no enlargement of the surface unit cell. As a matter of fact, the two viewpoints are equivalent: they predict the same stable surface configuration, and their difference is only semantic.

3.4.1. $Al_2O_3(0001)$. There have been numerous studies of the (0001) surface of α-Al_2O_3 single crystals. The surface is produced by cutting, polishing, and annealing, and gives rise to various reconstructed LEED patterns, according to the value of the annealing temperature

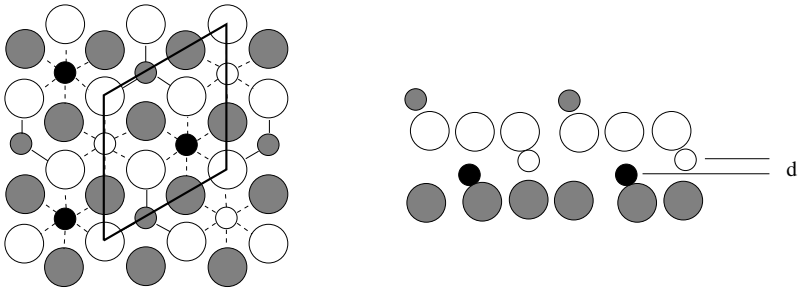

Figure 9. Top (a) and profile (b) views of a corundum crystal cut in the (0001) direction. The termination is assumed to be $M/O_3/M$. Small and large circles represent cations and anions, respectively.

T_{ann}. In ultrahigh vacuum, these include (1×1), $(\sqrt{3} \times \sqrt{3})R30^\circ$, $(2\sqrt{3} \times 2\sqrt{3})R30^\circ$, $(3\sqrt{3} \times 3\sqrt{3})R30^\circ$, and $(\sqrt{31} \times \sqrt{31})R \pm 9^\circ$, in order of increasing T_{ann} [105–107].

Although surface relaxations have been predicted for a long time, using different theoretical approaches [108–116], only recently has the structure of the unreconstructed (1×1) surface been quantitatively resolved [117–119]. It is terminated with a single Al layer, in agreement with electrostatic considerations. Strong relaxations take place which include a 51% contraction of the first interlayer distance, followed by smaller, but still non-negligible relaxations: +16%, −29%, and +20% for the next three interplanar spacings. The oxygen atoms in the second layer move laterally, so the Al–O bond length is only 4.5–6.1% contracted.

The structure of the intermediate reconstructions is not fully resolved, but the final $(\sqrt{31} \times \sqrt{31})R \pm 9^\circ$ surface structure is now well defined, thanks to GIXD experiments [120]. It can be viewed as a tiling of domains involving two metal Al(111) planes separated by a hexagonal network of domain walls, which can be obtained by evaporation of the two upper oxygen layers of the unreconstructed surface (figure 10). This description of the surface is consistent with an earlier model [105] and with the observation of the same reconstruction during the first stages of deposition of aluminium on a (1×1) α-$Al_2O_3(0001)$ surface. Although

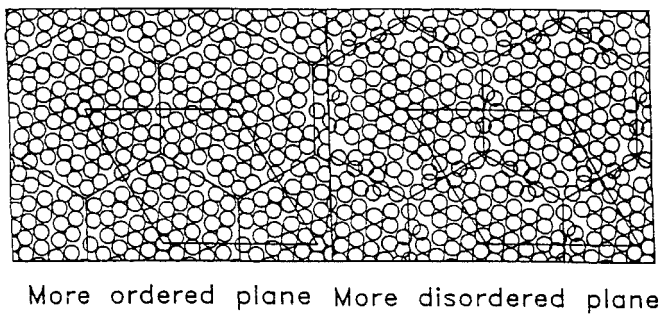

Figure 10. Several domains of the projected atomic structure of the α-Al_2O_3–$(\sqrt{31} \times \sqrt{31})R \pm 9^\circ$ reconstruction, where the unit cells as well as the domain walls are shown. The two constituent Al planes are shown separately, with evidence of one being much better ordered than the other. Numerical relaxation has shown that the ordered layer could be associated with the second layer and the more disordered one with the layer adjacent to the substrate. From reference [120].

this is not explicitly mentioned in the literature, this reconstructed surface should be charge compensated, if the starting (1×1) α-$Al_2O_3(0001)$ surface is itself compensated.

The energetics of stoichiometric slabs with (1×1) $Al/O_3/Al/\cdots$ and $O_3/Al/Al/\cdots$ terminations has been studied by a first-principles local density self-consistent-field embedded-cluster method [110]. The surface energy of the second slab (the polar one) is found to be nearly twice that of the first one (14 J m^{-2}, versus 7.4 J m^{-2}). The non-polar surface is insulating, with empty surface states derived from undercoordinated aluminium atoms. The position of the surface states differs according to the calculations, which do not agree on the existence of a surface gap narrowing. EELS experiments, on the other hand, find a surface gap width about one eV smaller than in the bulk [121]. No theoretical account of the electronic structure of the polar surface has been published to my knowledge.

Thin aluminium oxide layers have been synthesized using different preparation routes, either by direct oxidation of a metallic substrate containing Al, such as NiAl(110) [4, 122, 123] or $Ni_3Al(111)$ [124], or by deposition and oxidation of aluminium atoms on foreign substrates such as Mo(100), Ta(110) [125, 126], or Ru(001) and Re(001) [127, 128].

Thermal oxidation of NiAl(110) leads to the selective formation of Al_2O_3, which has a higher formation energy than NiO. The structure of thin films of 5 Å thickness is not α-Al_2O_3 as evidenced by HREELS spectra, but is more closely related to γ-Al_2O_3, with a proportion of the aluminium atoms located at tetrahedral sites. LEED and ISS (ion scattering spectroscopy) show that the surface is close packed and oxygen terminated.

Films grown on $Ni_3Al(111)$ [124] and at low thickness on Mo(100) [125] or Re [127] show similar evidence of the formation of γ-like Al_2O_3.

The existence of aluminium atoms at tetrahedral sites, together with the presence of an oxygen termination, in conflict with polarity arguments, have raised the question of the nature of these ultrathin films and their precise structure. *Ab initio* local density DFT calculations have led to the proposal of a model for a film 5 Å thick on top of an Al(111) substrate, in which the first oxygen layer in contact with the substrate is hexagonally packed as in the $O(1 \times 1)/Al(111)$ system. Aluminium atoms bind on top of those interfacial oxygens and to three oxygens in the layer above, thus adopting a tetrahedral environment. The outer oxygen layer is strongly relaxed inwards so as to make its atoms nearly coplanar with the aluminiums (figure 11). Surface polarity is thus strongly reduced [129].

The (0001) surface of sapphire α-Al_2O_3 can transform into the spinel-type Al_3O_4 structure under electron irradiation, as reported from atomic-resolution electron microscopy experiments [130].

3.4.2. $Cr_2O_3(0001)$. Thin films of chromium oxide have been produced either by thermal oxidation of a Cr(110) surface [4, 131–134] or by deposition and oxidation of chromium atoms on a Pt(111) substrate [135].

Films of Cr_2O_3 50–100 Å thick, resulting from the oxidation of Cr(110), display (1×1), $(\sqrt{3} \times \sqrt{3})$, and (1×1) LEED patterns sequentially as the temperature T is increased [136] (figure 12), with, in parallel, considerable changes in the EELS spectra. The two successive phase transitions are described as an order-to-order phase transition around 100 K and an order-to-disorder phase transition around 150 K, probably associated with movements of the chromium atoms on the surface, and possibly related to a magnetic effect. At low temperature, according to a quantitative LEED analysis [137], the outer layer consists of a single chromium layer as expected from electrostatic considerations, with the chromium atoms in registry with their bulk positions. Other possible surface sites are less consistent with experimental data and were shown to be less stable by molecular dynamics simulations using a fully ionic model. Strong inward relaxations are found for the two first interlayer distances (-38% and -21%),

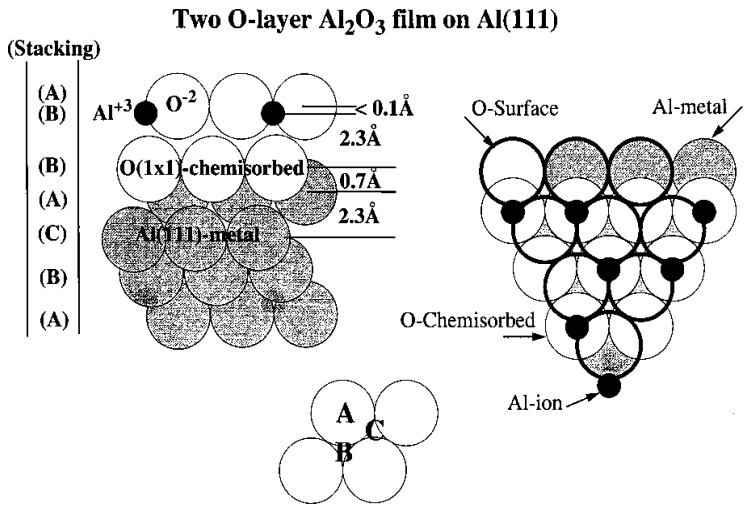

Figure 11. Side and top views of the most favoured geometry of a 5 Å thick Al_2O_3 film on top of an Al(111) substrate, with tetrahedral Al ions atop oxygens chemisorbed in the fcc hollows of the Al(111) surface, with a stacking fault at the second oxygen layer. From reference [129].

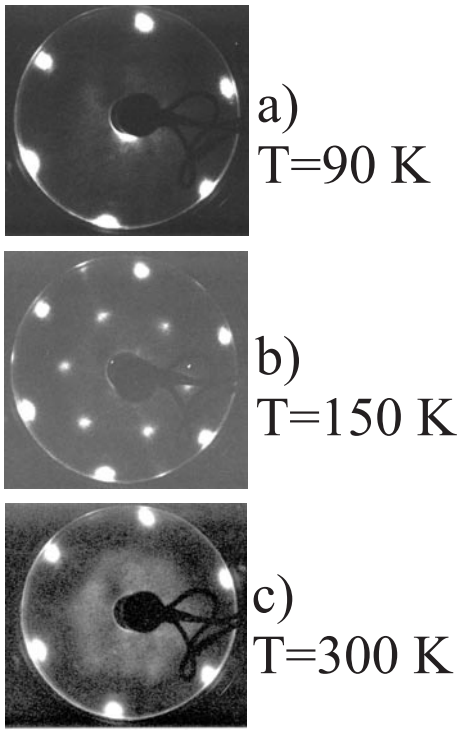

Figure 12. A series of LEED patterns of Cr_2O_3/Cr(110) taken at different temperatures. From reference [4].

concomitant with a reduced ionicity of the ions at the surface. This structure has been checked by quantum chemical *ab initio* calculations in a study of surface d–d excitations and the reduction of ionicity at the surface has been confirmed [137, 138].

On Pt(111) [135], chromium oxide films present a well-ordered p(2 × 2) structure below

2 ML which is attributed to the growth of metastable spinel $Cr_3O_4(111)$, while at higher coverage a $(\sqrt{3} \times \sqrt{3})R30^\circ$ structure appears, which is attributed to the formation of either a γ-Cr_2O_3 phase or a reconstructed α-$Cr_2O_3(0001)$ surface [139]. This growth sequence presents some degree of similarity with the growth of iron oxide films on the same substrate, except, in the first stages of growth, for the absence of chromium monoxide, which is thermodynamically unstable.

A GIXD study, performed on a $Cr_2O_3(0001)$ single-crystal surface [140], gives a slightly different picture of the surface structure and provides some explanation of the observed phase transitions. The data give evidence for a disordered arrangement of the top-layer chromium atoms, with only a 2/3 occupation probability, and a 1/3 probability of chromium atoms occupying distorted octahedral interstitial sites below the oxygen top layers (sites which are unoccupied in the bulk). A very small relaxation of the top layer (-6%) is deduced, at variance with the LEED results. The ordering of the interstitial sites could explain the $(\sqrt{3} \times \sqrt{3})R30^\circ$ structure observed in the 100–150 K temperature range. It seems that this structural arrangement increases the dipole moment of the surface unit, and it is not obvious at this point why it corresponds to a low-energy configuration.

Water on $Cr_2O_3(0001)/Cr(110)$ adsorbs molecularly, except at defect sites [141].

Besides those already quoted, several modellizations of the α-$Cr_2O_3(0001)$ surface have been performed. The *ab initio* Hartree–Fock method has been used to determine the atomic and electronic ground-state configuration of the surface. The Cr-terminated surface is found to be stable and strongly relaxed inwards (-50%), without lateral displacements of the underlying oxygens. Ionicity is hardly changed with respect to that of the bulk, and it is argued that this strong relaxation is driven by the necessity to decrease the net charge of the surface plane [142]. *Ab initio* embedded-cluster calculations of the adsorption of water on α-$Cr_2O_3(0001)$ surfaces have furthermore shown that among the four possible locations of the chromium atoms in the outer layer, only the 'bulk' one is consistent with molecular adsorption of water [143]. Classical molecular dynamics simulations have also predicted that the oxygen termination of α-$Cr_2O_3(0001)$ can have a high probability of occurring due to the presence of superficial lattice defects [144].

3.4.3. $V_2O_3(0001)$. V_2O_3 films have been grown on a variety of substrates ranging from metallic Au(111) [145] and Cu(100) [146], to insulating $TiO_2(110)$ [147–149] or $Al_2O_3(0001)$ [150–152]. Like titanium or iron, vanadium exists in several oxidation states, and various stoichiometries may be produced depending upon the preparation conditions. Among them, V_2O_3 and VO_2 have aroused much interest, because they display a metal–insulator transition, considered to be of the Mott–Hubbard type.

Deposition and oxidation of vanadium atoms onto an Au(111) substrate leads to growth, in a simultaneous multilayer mode, of a well-ordered $V_2O_3(0001)$ film [145], displaying a $(\sqrt{3} \times \sqrt{3})$ LEED pattern. This corresponds to the smallest lattice mismatch between V_2O_3 and the substrate.

On $TiO_2(110)$, deposition of vanadium in an O_2 atmosphere results in the formation of lower oxides, that interact weakly with the substrate [147]. On the unreconstructed (1×1) substrate, V_2O_3 has been identified by several vacuum surface analytical techniques [148]. A synchrotron study furthermore showed that V_2O_3 grows in a two-dimensional fashion, without any long-range order, probably via a simultaneous multilayer growth mode [149].

V_2O_3 also grows epitaxially on an $Al_2O_3(0001)$ film supported on Mo(110). Only short-range order exists in the film and the vanadium atoms are in an octahedral environment [152]. Electronic structure measurements have been performed to investigate the mechanism of the metal–insulator transition [151], as for a $V_2O_3(0001)$ single-crystal surface [153].

3.4.4. $Fe_2O_3(0001)$. Haematite Fe_2O_3 single crystals exhibit unreconstructed or reconstructed (0001) surfaces, depending upon the conditions of surface preparation [95, 154, 155]. In particular, high-temperature annealing produces a reduction of the surface and the appearance of LEED patterns characteristic of a superficial $Fe_3O_4(111)$ film.

Growth of thin films of α-Fe_2O_3 has been reported on Mo(100) [71], Pt(111) [67, 69, 156], α-Al_2O_3 [73, 87, 91, 102, 157–161] substrates, as well as on Pt(111)-covered α-Al_2O_3, to improve the lattice mismatch [90]. The latter is 4.6% on Pt(111) and 5.7% on α-Al_2O_3. The hexagonal symmetry of the substrates favours the formation of α-Fe_2O_3, while on cubic substrates, such as MgO(100), the metastable maghemite γ-Fe_2O_3 is obtained [102] (see section 3.3.1).

On Pt(111), the α-$Fe_2O_3(0001)$ surface is unreconstructed [69], and is characterized by an electronic structure [67] very similar to that of a single-crystal surface [162]. The nature of the surface termination is a function of the oxygen pressure p_{O_2} [163]. In particular, at p_{O_2} of the order of 1 mbar, the O termination is stabilized, while, in the range $10^{-4} < p_{O_2} < 10^{-1}$, Fe and O terminations coexist. This is in agreement with the results of *ab initio* LSDA (local spin-density approximation) calculations [164], which show that, despite polarity effects, the difference in surface energy between the two terminations can be cancelled out by chemical potential effects in the estimation of the surface Gibbs free energy (figure 13). Relaxation effects on both terminations are found to be very large: -57% for the Fe–O interlayer distance on the Fe termination, and -1% and -79% for the first two interplanar distances on the O termination, accompanied by a rotation of the surface oxygen atoms. The first number compares with the values +1% and -49% obtained in pair potential approaches, not allowing or allowing for some ion polarization, respectively [108, 165].

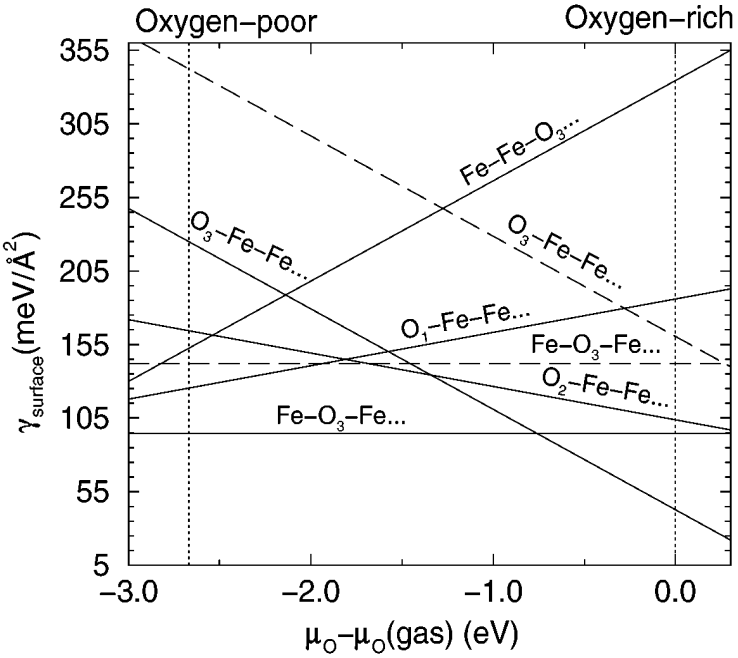

Figure 13. Surface energies of different $Fe_2O_3(0001)$ surface terminations. μ_O(gas) is the chemical potential per oxygen atom of molecular O_2. The allowed range of $\mu - \mu_O$(gas) is indicated by the vertical dotted lines. Solid lines show results for relaxed geometries, and dashed lines give, for comparison, results for unrelaxed surfaces. From reference [164].

On α-Al_2O_3(0001) substrates, α-Fe_2O_3(0001) films were grown by evaporating Fe from a Knudsen cell onto the substrate and simultaneously oxidizing the metal [91, 161]. Layer-by-layer growth is observed up to a critical thickness of six Fe/O_3/Fe repeat units, beyond which growth becomes three dimensional. In the first regime, an anomalous expansion of the film lattice parameter with respect to those of both bulk α-Fe_2O_3 and α-Al_2O_3 takes place. A formation of α-Fe_2O_3(0001) with a random distribution of Fe^{3+} ions, rather than of a wustite-type FeO layer [73] (section 3.2.4), was suggested, but no explanation of the lattice expansion was proposed.

When an oxygen plasma source is used for the oxidation of Fe atoms deposited on α-Al_2O_3(0001) or Pt(111)/α-Al_2O_3(0001) substrates, and under specific Fe/O flux ratios, unreconstructed α-Fe_2O_3(0001) films are obtained, with Fe termination, as suggested by electron-counting rules [87, 90]. The relaxations of the outermost layers were determined by XPD [166]: the values of -41%, $+18\%$, -8%, and 47% are in reasonable agreement with theoretical estimates from LSDA calculations [164] (-57%, $+7\%$, -33%, $+15\%$), at least for the outermost interlayer distances. Below three monolayers [157], the film is considered as compressionally strained and fully stoichiometric, with a badly distorted interfacial layer commensurate with the substrate, at variance with the interpretation given in reference [161].

3.4.5. Summary. The polar instability of the (0001) face of corundum crystals depends upon the nature of the termination. Unreconstructed configurations are currently observed on M/O_3/$\cdots$-terminated surfaces, with no anomalies† in the electronic structure, but with strong relaxations of the outer layers. The unreconstructed polar oxygen termination of Fe_2O_3, on the other hand, has been observed under oxidizing conditions, in agreement with theoretical predictions. However, an analysis of its electronic structure, which could shed some light on the mechanism of charge compensation, is lacking.

3.5. The wurtzite (0001) and (000$\bar{1}$) surfaces

ZnO can crystallize in the hexagonal wurtzite structure, in which each zinc (oxygen) atom is located at the centre of an oxygen (zinc) distorted tetrahedron. Such coordination is characteristic of rather covalent compounds and indeed ZnO is at the borderline between semiconductors and insulators. When cut along the polar (0001) or (000$\bar{1}$) directions, the crystal exhibits a Zn/O/$\cdots$ stacking of the hexagonal type AbBaA$\cdots$ (capital letters for the Zn atoms, for example), and the surface is Zn terminated or O terminated, respectively. The outer layer may consist of either A (a) or B (b) planes, which are rotated by 180° with respect to one another. The surface atoms are threefold coordinated (figure 14). In the bulk, the interplane distances are equal to $R_1 = 0.61$ Å and $R_2 = 1.99$ Å inside and in between the double layers, respectively. As a consequence, the condition for stabilization of the polar orientation requires surface charge densities equal to $\sigma' = \sigma R_2/(R_1 + R_2) \approx 0.765\sigma$.

The (0001) and (000$\bar{1}$) surfaces of single-crystal ZnO are unreconstructed or reconstructed depending upon the surface preparation conditions. In particular, both cleaved and polished surfaces subjected to ion bombardment below 600 °C exhibit a p(1 × 1) LEED diagram. Annealing at higher temperature may lead to (2 × 2), ($\sqrt{3} \times \sqrt{3}$), (3 × 3), or ($4\sqrt{3} \times 4\sqrt{3}$) reconstructions, some of them being possibly due to surface contamination [167–172]. The diffraction patterns of the unreconstructed surface present a sixfold rather than the threefold symmetry expected from ideal bulk truncation. This was attributed to the presence of double

† By this, we mean that there is no change in the formal charges of the surface atoms. For simple oxides, like Al_2O_3, this implies in particular that oxygen-derived electronic states are filled and cation-derived states empty, whether in the bulk or at the surface.

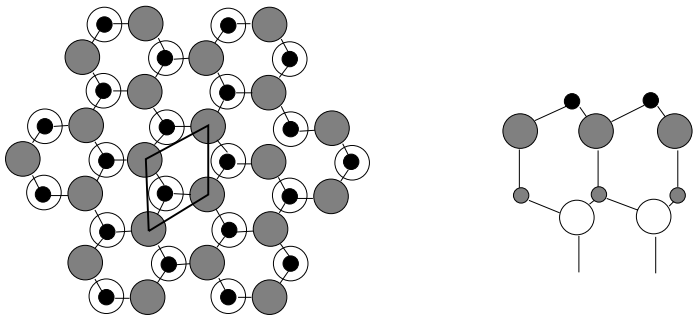

Figure 14. A top view (a) and a profile view of the wurtzite (0001) surface. Large and small circles represent oxygen and zinc atoms, respectively.

steps on the surface [172–174], which were indeed visualized in STM experiments, although no atomic resolution could be achieved [175, 176].

The atomic structure of the unreconstructed surfaces was quantitatively investigated by several techniques, including LEED [177], XPD [178, 179], ISS [174], and GIXD [180]. By performing a dynamical LEED analysis of the unreconstructed (0001) Zn face and $(000\bar{1})$ O faces, Duke and Lubinsky [177] found a value of the first interplanar distance of 0.607 Å, for the former, and 0.8 Å, for the latter. They incorrectly inferred relaxation values of -0.2 Å and ≈ 0 Å, respectively, using, as the bulk reference, the wrong value 0.807 Å. Relaxation effects on the oxygen-terminated face [178, 179] and on the zinc face [178] were also measured by means of XPD, and were shown to be approximately zero. The same conclusion for the oxygen termination was reached using angle-dependent low-energy alkali-ion scattering [174]. Recently, both terminations have been reinvestigated by means of GIXD [180], for unreconstructed samples obtained after several cycles of Ar^+ bombardment and annealing at 800 °C. The Zn surface presents a +0.05 Å outward relaxation associated with a 0.75 occupancy of the Zn sites in the outer layer, as expected from electrostatic considerations. The O termination is relaxed inward by -0.03 Å, and the occupancies of both the outer and the underlying layers are different from those for the bulk, consistently with an earlier suggestion based on work-function measurements [181].

The electronic structure of the unreconstructed faces has been addressed by angle-resolved photoemission [182, 183] and total-current spectroscopy [184], which showed surface-induced features in the occupied part, as well as in the unoccupied part of the DOS (figure 15).

Theoretical predictions for the atomic structure, electronic structure, and/or stability of the polar faces of ZnO have relied on electrostatic arguments [6], or embedded-cluster [185–187] or slab calculations [188, 189]. Using electrostatic considerations, Nosker *et al* [6] have predicted that surface stability may be reached either by removing 1/4 of the outer atoms on each termination, leading to a reconstructed configuration, or by faceting, the latter process yielding a lower surface energy. Despite finite-size effects, DV-X_α calculations on clusters [185] have shown that a spontaneous charge redistribution takes place on the stoichiometric terminations, as expected from the electrostatic criterion. It was attributed to a modification of the iono-covalent bonding on the Zn face, and to partial filling of surface states on the oxygen face. Part of this picture was confirmed by slab calculations based on the density functional theory in the generalized gradient approximation [189], which furthermore predicted values of the relaxation for the outer layer of -0.15 Å and -0.25 Å on the fully stoichiometric Zn and O

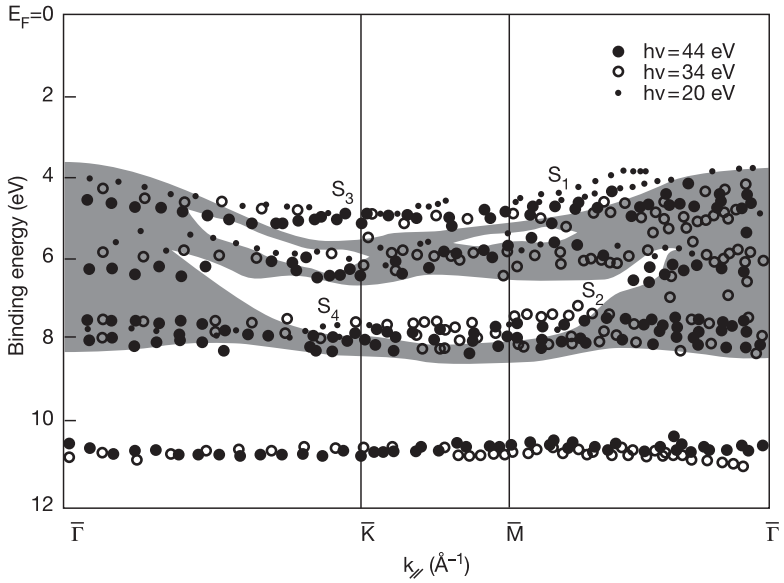

Figure 15. The surface band structure as obtained from angle-resolved photoemission experiments on ZnO(0001). The hatched area shows the projection of bulk states onto the surface Brillouin zone. From reference [183].

terminations, respectively. Optimized values of 0.43 Å and 2.06 Å for the two outer interlayer distances on the Zn face and 0.34 Å and 2.07 Å for the O face are also quoted in the literature as unpublished theoretical results [188], but it is not obvious that the Harris–Foulkes method used in this study allows one to reach full self-consistency between charges and electrostatic potentials on polar surfaces.

To summarize, early observations of unreconstructed ZnO(0001) or $(000\bar{1})$ surfaces, assumed to be fully ordered, with no anomalous electronic structure, seemed puzzling, since they contradict the electrostatic criterion. The recent GIXD study which finds partial occupancy of surface sites, without long-range order of the surface vacancies, partly clarifies the problem and should be confronted with numerical simulations in the future.

3.6. Perovskite ABO_3 surfaces

The perovskite ABO_3 structure possesses a cubic unit cell with the A cations at the cube vertices, the B cations at the cube centre, and oxygens at the face centres. As represented in figure 16, the (100) surface can exhibit either an SrO or a TiO_2 termination. The alternating layers are equidistant ($R_1 = R_2$), and I mentioned in the introduction that they are not neutral. This surface is the prototype of what we called 'weakly polar surfaces' [190]. The electrostatic condition for surface stability is $\sigma' = \sigma/2$. The (110) and (111) orientations are polar with equidistant layers ($R_1 = R_2$) in their repeat units, of the B/AO_3, and O_2/ABO type, respectively. The layers formally bear charge densities equal to ± 4 per surface unit cell, and require compensating charges equal to ± 2.

3.6.1. The (100) surface. Electronic states at the (100) (1×1) surface of single-crystal $SrTiO_3$ have been studied by means of photoemission and electron energy-loss spectroscopy. There is no evidence of deep surface states in the gap when the surface is defect free [191, 192].

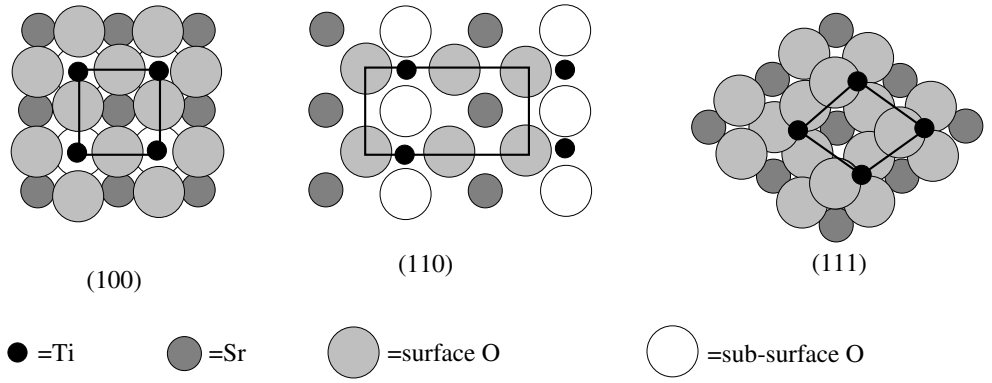

Figure 16. The (100), (110), and (111) surface orientations of $SrTiO_3$. The stackings are as follows: $TiO_2/SrO/\cdots$, $O_2/SrTiO/\cdots$, and $Ti/SrO_3/\cdots$, respectively.

Covalency of the Ti–O bond is enhanced at the surface [193], and surface Ti 3p levels present a 2 eV chemical shift with respect to the bulk [194]. It was found that the surface easily presents a mixture of the SrO and TiO_2 terminations [195]. A value of 6 eV for the local gap on SrO-rich terraces was measured by STS (scanning tunnelling spectroscopy) [196]. Determinations of the surface relaxations on both terminations were made by quantitative LEED analysis [197] and RHEED and XPD measurements [198, 199]. They agree on the existence of a surface rumpling with the oxygen atoms pulled outwards, but not quantitatively on the interlayer spacings.

The surface relaxation has been calculated by various theoretical approaches, ranging from classical atomistic methods [200, 201] to first-principles calculations in a slab geometry [202, 203]. The surface rumpling is reasonably accounted for, but all calculations predict an inward relaxation of the outermost layer on the TiO_2 termination, in contradiction with both types of experiment.

Particular attention has been focused on the energy position of the surface states. The first non-self-consistent calculations found some surface states located deep in the gap [204, 205]. All subsequent self-consistent calculations have contradicted this prediction, whether they were based on cluster models [206] or on unrelaxed [207] or relaxed [202, 203] slabs (figure 17), in agreement with photoemission and electron-loss spectroscopy results [3]. When calculated [202, 203], the surface energy is rather low, an indication that no surface instability arises.

On defective surfaces, for example after Ar bombardment, surface states appear in the band-gap region [193]. They were attributed to Ti^{3+}–O–vacancy complexes [192]. When exposed to high temperatures in a reducing environment, besides the expected appearance of oxygen vacancies, changes in cation concentrations and in cation-to-cation ratios take place, which were quantified by Rutherford backscattering and Auger electron spectroscopy [208, 209]. STM evidenced the formation of Ruddlesden–Popper phases $Sr_{n+1}Ti_nO_{3n+1}$ as a way to accommodate the non-stoichiometry [209, 210]. Various reconstructions have been observed on vacuum-annealed surfaces: (2×2) [211], $(\sqrt{5} \times \sqrt{5})$R26.6° [212–215], c$(2 \times 2)$ [216]. They were attributed to an ordering of oxygen vacancies, the latter reconstruction being possibly due to Ca segregation on the surface.

Simulations of oxygen vacancies agree on the existence of defect states in the gap [206, 207, 217]. $(\sqrt{2} \times \sqrt{2})$ and $(\sqrt{5} \times \sqrt{5})$R26.6° reconstructed surfaces with one oxygen vacancy per unit cell have a metallic character [207, 217]. The calculated interaction energies of vacancies depend not only upon the termination, but also upon the inequivalent positions of

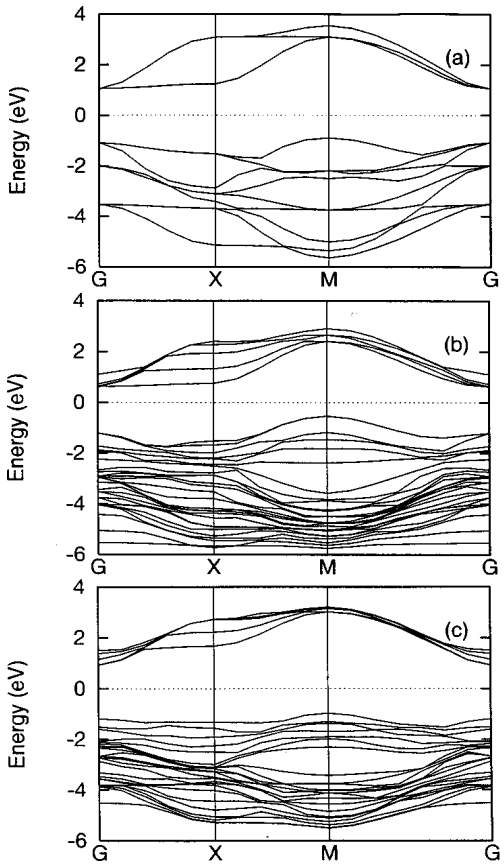

Figure 17. Calculated band structures for $SrTiO_3$: (a) surface-projected band structure; (b) TiO_2 terminated; (c) SrO terminated. The zero is the Fermi level determined by a Gaussian smearing of 0.2 eV. From reference [203].

the vacancy pair at first-neighbour sites, on the TiO_2 face [10]. Due to the lack of knowledge of the precise surface stoichiometry in the experiments, it is at present difficult to propose a structure for the reconstructed surfaces.

3.6.2. The (111) and (110) surfaces. The $SrTiO_3$(111) [218–221] and (110) surfaces [222–224] and the $BaTiO_3$(111) surface [225] have been produced and studied. At variance with those performed on rock-salt oxides, many of these investigations suggest that one can obtain non-reconstructed quasi-planar polar surfaces.

A (111) face prepared by Ar bombardment and subsequent annealing below 1100 °C exhibits a (1 × 1) structure [218, 219], with the top layer being of either SrO_{3-x} or Ti composition. There is no evidence of surface states in the bulk-projected band gap. In references [219, 221], surface atoms with anomalous charge states were detected by core-level spectroscopy.

Similarly, STM observations on $BaTiO_3$(111) [225] showed that (1 × 1) faces may be produced under specific preparation conditions—annealing under an oxygen atmosphere and at temperatures that are not too high. However, no precise determination of the layer stoichiometry was performed.

The $SrTiO_3(110)$ surface displays a variety of reconstructions, such as $c(2 \times 6)$, according to LEED [222] and STM [224] observations, under reducing conditions. Samples annealed at 800 °C and then exposed to an oxygen-rich atmosphere at room temperature [222] have a zero density of states at the Fermi energy and a (1×1) LEED pattern. XPS [222, 223] spectra of Ti core levels reveal the existence of Ti^{3+} and Ti^{2+} species.

The atomic and electronic structures of $SrTiO_3(111)$ and (110) (1×1) surfaces have been investigated using a total-energy, semi-empirical Hartree–Fock method [226, 227]. Terminations of various stoichiometries, whether compensated or not, exhibit strong electron redistributions, which suppress the macroscopic component of the dipole moment (figure 18). For stoichiometric non-compensated surfaces (e.g. SrO_3 or Ti(111) layers), this is an expected result, but redistributions are also present on stoichiometry-compensated surfaces (e.g. SrO_2 or TiO(111) layers), leading to an anomalous filling of surface states and anomalous charge states for some surface atoms. All terminations were found to be insulating, a result attributed to the specific value ± 2 of the compensating charges, which allows the complete filling of one surface state per unit cell. The average surface energies were found to be rather low, consistently with the possibility of fabrication of the planar (1×1) $SrTiO_3(111)$ and (110) surfaces. The relative stability of terminations of different stoichiometries was calculated as a function of oxygen chemical potential and it was anticipated that non-stoichiometric reconstructions are not necessarily efficient mechanisms for stabilizing the surface.

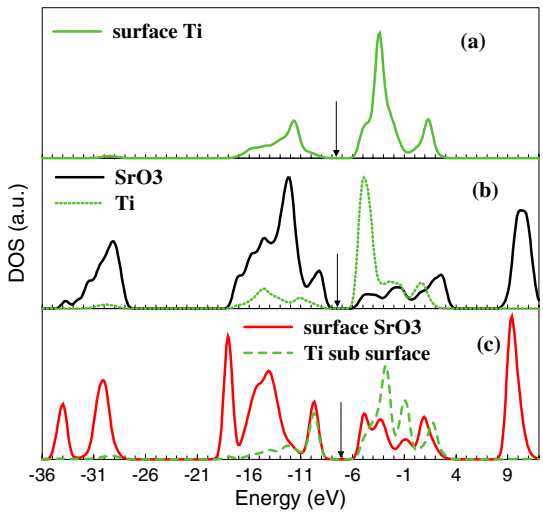

Figure 18. The local density of states on a $SrTiO_3(111)$ slab containing stoichiometric SrO_3 and Ti layers: (a) the Ti-termination-projected DOS; (b) the bulk DOS; (c) the SrO_3-termination-projected DOS; all DOS have been convoluted with a 0.5 eV wide Gaussian function. Note the enhanced contribution of the valence DOS on the outer Ti on the Ti termination and on the sub-surface Ti on the SrO_3 termination, and the overall insulating character of the surface layers (the Fermi level is indicated by an arrow). From reference [227].

3.6.3. Summary. The polar instability of the $SrTiO_3(100)$ surface is very weak. There is no evidence of anomalous filling of electronic states on the unreconstructed face, which can be currently obtained. The (110) and (111) faces, on the other hand, can also be produced unreconstructed, but the precise stoichiometry of the surface layers has not yet been determined. However, the structure is such that ordered vacancies in the surface layers are compatible with

(1 × 1) diffraction patterns. The mechanism of stabilization is thus not obvious at present and it would be interesting, in the future, to assess whether it is due to the presence of disordered surface vacancies or ordered vacancies, or whether the stoichiometric surface, with a complete filling of cation-derived surface states, has indeed a low surface energy, as predicted theoretically.

4. Discussion

After a presentation of the three analytical models allowing an approximate account to be given of the electron distribution in iono-covalent materials, we will discuss the efficiency of various processes invoked in the literature as yielding charge compensation. Finally, we will summarize the different scenarios leading to a cancellation of polarity.

4.1. Models of electronic structure in iono-covalent materials: application to polar surfaces

Oxide compounds have a noticeable degree of ionicity in their metal–oxygen bonding. For this reason, a model in which they are assumed fully ionic is usually considered as a good zeroth-order approximation. This is well exemplified in the field of polar surfaces. On the other hand, due to the earlier development of the physics of compound semiconductor surfaces, concepts suited to their specific electronic characteristics—e.g. the directional overlap between sp_3 orbitals in the tetrahedral zinc-blende or wurtzite structures, the existence of 'dangling bonds', etc—have been developed and this has led to the expression of the auto-compensation principle and the electron-counting model. It turns out that neither of these two models is satisfactory for treating polar oxide surfaces, while a description in terms of electron transfer per bond allows one to make a bridge between the two limits and can account for the metal–oxygen bonding for the whole range of ionicities.

4.1.1. The ionic model. In the limit of full ionicity, formal charges are assigned to bulk as well as to surface atoms: +2 for Mg, Sr, Ba; +3 for Al; +4 for Ti in TiO_2 or $SrTiO_3$; −2 for O; etc. This model is often used successfully to assess whether the bulk repeat unit bears a non-zero dipole moment, and to predict stable surface configurations.

For example, it correctly tells us that a bulk truncated MgO or NiO(111) termination does not fulfil the stability criterion (equation (2.1)), while an octopolar reconstructed p(2 × 2) configuration does, in agreement with experimental observation. Similarly, it correctly predicts that the corundum (0001) surface terminated by a single metal layer is stable.

This model applies well to highly ionic materials, but its use cannot be justified for more covalent compounds. For example, according to the model, the surface energies of stoichiometric $SrTiO_3$ and $BaTiO_3$(111) and (110) surfaces should be infinite, as should those of the oxygen or iron bilayer terminations of α-Fe_2O_3(0001), in contradiction with both experiment and *ab initio* calculations. The estimation of reliable surface charges thus seems a necessary requirement in these cases, but it is beyond the capabilities of the model.

In addition, as we have already mentioned, the ionic model may even give wrong predictions on the nature (polar or not) of a surface, as in the case of $SrTiO_3$(100)

4.1.2. The electron-counting model and the auto-compensation principle. In the world of tetrahedral semiconductor compounds, a criterion for the stability of polar surfaces has been stated, in terms of specific fillings of dangling bonds. In these materials, an overlapping between sp_3 hybrids localized on neighbouring atoms takes place, and the

valence and conduction bands correspond to their bonding and anti-bonding combinations, respectively. A surface dangling bond may be viewed as an sp_3 atomic orbital which remains unpaired due to surface bond breaking. The criterion is referred to as the auto-compensating model [228, 229].

This model states that a surface is stable if valence band states (bonding orbitals) are completely filled and conduction band states (anti-bonding orbitals) completely empty. For tetrahedral semiconductor compounds, this amounts to saying that anion-derived and cation-derived dangling bonds must be filled and empty, respectively. The existence of a gap in the band structure stabilizes the occupied surface states and destabilizes the unoccupied ones, resulting in a net lowering of the surface energy.

The model most widely used in this field to estimate the surface-state filling is the electron-counting model. It assumes that the participation of each atom in a given bond is proportional to its valence in the bulk, and stays unchanged at the surface. This dictates the occupation of the dangling bonds. For example, in bulk GaAs, each atom shares its three (Ga) or five (As) outer electrons between the four surrounding bonds. From the two electrons which fill each bonding orbital, it is thus assumed that 3/4 come from Ga and 5/4 from As. On the unreconstructed Ga-terminated (111) surface, for example, a Ga atom gives $3 \times 3/4$ electrons to the three back-bonds and 3/4 electrons remain in the dangling bond. This does not fulfil the auto-compensation principle, which however is obeyed if 1/4 of atoms are removed from the surface layer. A similar situation occurs for the (100) surface (figure 19).

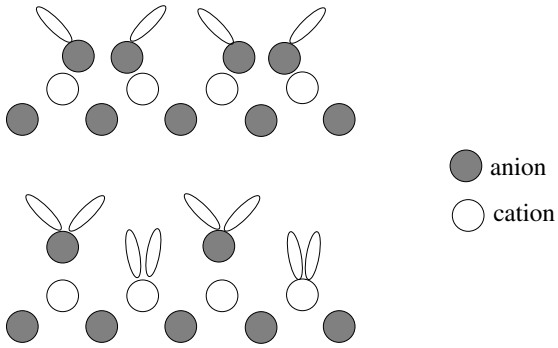

Figure 19. A schematic side view of an anion-terminated GaAs(100) surface reconstructed with (a) dimers and (b) vacancies of surface atoms. Filled anion dangling bonds (shaded) and empty cation dangling bonds (open) are represented.

It has been realized that, at polar surfaces, the condition of auto-compensation implies that equation (2.1) is fulfilled, and the surfaces are then said to be 'charge neutral' [230].

Later, the auto-compensation principle was generalized to apply to mineral surfaces [231]. In these compounds, usually, the number of electrons involved in each bond is less than 2. For example, in MgO, there are eight valence electrons per formula unit (two from Mg and six from O, if the oxygen 2s and 2p electrons are included) distributed in six bonds, which amounts to 4/3 electrons per bond. In the generalized version of the auto-compensation principle, the electron number per bond at the surface is required to be the same as in the bulk. This principle has been applied for example to α-Al_2O_3(0001) [232], Fe_3O_4(100) [89, 91–93], and α-Fe_2O_3(0001) [87, 90].

This generalization may be useful in a number of cases. However, the vocabulary taken from the physics of semiconductors is highly unsuitable for oxides, because, in most cases, dangling bonds have no physical significance. The conservation of the number of electrons per

bond between bulk and surface is also not a well-founded assumption. In addition, it would be very difficult to extend this approach to ternary systems. The electron counting in bulk $SrTiO_3$, for example, gives a number of electrons per bond averaged over Ti–O and Sr–O bonds, but no information on the electron distribution in each bond separately.

4.1.3. The bond-transfer model. We have recently proposed a model [233] which provides an approximate description of charge distribution in simple charge-transfer oxides. It is valid over the whole range of ionicities and makes no assumption on the nature of the orbitals involved in the bonding.

This model relies on a tight-binding approach, in which the eigenstates of the system are expanded in a valence atomic orbital basis set. In this orbital basis set, the matrix elements of the diagonal (H_{D}) and non-diagonal (H_{ND}) parts of the Hamiltonian are the effective atomic orbital energies ϵ, and the resonance integrals β, assumed to be non-zero if the overlap between orbitals on two neighbouring sites is non-vanishing. The local density of states (LDOS) on the various atoms is obtained from the imaginary part of the trace of the Green's operator $G^+(E)$, and charges may be subsequently determined by integration of the LDOS up to the Fermi level. $G^+(E)$ is given as a function of H_{ND} and of the Green's operator $G_0^+(E)$ associated with H_{D}, by Dyson's equation. The summation of bubble diagrams up to infinite order yields a self-energy-type approximation for $G^+(E)$, which is then diagonal in the atomic orbital basis set. Bubble diagrams represent hopping processes along closed paths, in which an electron, located on a given atomic orbital Xλ, hops onto a neighbouring atom and then comes back to Xλ. They provide a correct description of the *local* anion–cation hybridization inside a small cluster which includes the central atomic orbital Xλ and all the neighbouring orbitals with non-vanishing overlap with Xλ. Long-range band effects, on the other hand, are neglected, which means for example, that, for an insulator, the valence and conduction bands are made up of several 'delta' peaks with zero width; however, the first and second moments of the LDOS are exactly treated.

It can then be proved, starting from the ionic limit in which anions and cations bear formal charges (Q_{A}^0 and Q_{C}^0, respectively), that the sharing of electrons due to orbital overlap is fully described by quantities $\Delta_{\mathrm{A}_i\mathrm{C}_j}$, defined for each bond. For simple insulating oxides with a completely filled oxygen-derived valence band, the charges on an anion A_i or a cation C_j are expressed as

$$Q_{\mathrm{A}_i} = Q_{\mathrm{A}}^0 + \sum_{\mathrm{C}_j} \Delta_{\mathrm{A}_i\mathrm{C}_j} \qquad Q_{\mathrm{C}_j} = Q_{\mathrm{C}}^0 - \sum_{\mathrm{A}_i} \Delta_{\mathrm{A}_i\mathrm{C}_j}. \tag{4.1}$$

The summation runs over the first-neighbour atoms. Each transfer Δ, being related to a *bond*, concerns *two* atoms and appears in the expression for their charges. This description presents some degree of analogy with the bond orbital model [234]. We have used it for a thorough discussion of the Ti–O bonding and of screening effects in small $(TiO_2)_n$ clusters, and the rutile $TiO_2(110)$ surface and bulk [235].

Moreover, the model can treat the case of partial filling of a valence or conduction state—which can take place on polar surfaces. For example, if a conduction band state, derived from a cation $\mathrm{C}_0\mu_0$ orbital, has a filling factor f, the charges on C_0 and its neighbouring atoms become equal to

$$Q_{\mathrm{C}_0} = Q_{\mathrm{C}}^0 - \sum_{\mathrm{A}_i} \Delta_{\mathrm{A}_i\mathrm{C}_0} - f\left(2 - \sum_{\mathrm{A}_i} \delta_{\mathrm{A}_i\mathrm{C}_0}\right) \qquad Q_{\mathrm{A}_i} = Q_{\mathrm{A}}^0 + \sum_{\mathrm{C}_j} \Delta_{\mathrm{A}_i\mathrm{C}_j} - f\delta_{\mathrm{A}_i\mathrm{C}_0} \tag{4.2}$$

with $\delta_{\mathrm{A}_i\mathrm{C}_0}$ the electron transfer between the $\mathrm{C}_0\mu_0$ orbital and the A_i neighbours.

The electron transfers per bond are given in the theory by

$$\Delta_{A_iC_j} = \left[\beta^2_{A_i\lambda,C_j\mu}\Big/\left(\sum_{A_k\nu}\beta^2_{A_k\nu,C_j\mu}\right)\right]\left(1-(\epsilon_{C_j}-\epsilon_{A_i})\Big/\sqrt{(\epsilon_{C_j}-\epsilon_{A_i})^2+4\sum_{A_k\nu}\beta^2_{A_k\nu,C_j\mu}}\right) \tag{4.3}$$

as a function of the resonance integrals $\beta_{A_i\lambda,C_j\mu}$ and the local atomic orbital energies ϵ_{C_j} and ϵ_{A_i}; similar expressions hold for $\delta_{A_iC_0}$ in equation (4.2), without a summation over μ. As expected, $\Delta_{A_iC_j}$ goes to zero in the fully ionic limit (zero resonance integrals) and increases when the degree of covalency $\beta_{A_i\lambda,C_j\mu}/(\epsilon_{C_j}-\epsilon_{A_i})$ of the bond increases.

When atoms are in a highly symmetric environment, equation (4.1) reduces to a very simple expression, which involves the atom coordination number and a very small number of parameters Δ. For example, in bulk MgO, the six bonds surrounding each atom are equivalent. They are associated with a single Δ value, so the valence electron numbers N and charges Q read

$$\begin{aligned} N_{Mg} &= 6\Delta & Q_{Mg} &= 2-6\Delta \\ N_O &= 8-6\Delta & Q_O &= -2+6\Delta. \end{aligned} \tag{4.4}$$

The Madelung potential acting on surface atoms differs from its bulk counterpart, and this induces shifts in the effective atomic orbital energies [1]. Surface relaxation may also modify the values of the resonance integrals with respect to the bulk. The $\Delta_{A_iC_j}$ in the bulk and at the surface are thus usually different [235] (figure 20). Moreover, when the cancellation of the macroscopic dipole moment of a polar surface requires the filling of a conduction state or the depletion of a valence state, since, usually, those states are derived from orbitals on atoms with the lowest coordination number [236, 237], the electron counting can be redone taking into account the actual position of the Fermi level.

Actually, for understanding the mechanisms at work to cancel polarity, it will never be necessary to know quantitatively the values of the electron transfers per bond $\Delta_{A_iC_j}$. It is the principle of electron sharing per bond which is the key ingredient for the discussions of the next section.

4.2. Discussion of surface processes relevant for cancelling the polarity

The application of the bond-transfer model to polar surfaces allows one to analyse the efficiency of various processes suggested to cancel the polarity. We will successively discuss the importance of surface relaxation, the change of covalency in the outer layers, the filling of surface states, and the change in stoichiometry, in the context of semi-infinite polar surfaces. In the last section, we will focus on some specificities of ultrathin films.

4.2.1. Surface relaxation. It is often thought that surface relaxation takes an important role in the process of stabilization of polar surfaces, especially for open surfaces, where large relaxations are observed. Actually, two aspects of the problem should be distinguished.

First, as far as the cancelling of polarity is concerned, it is important to realize that surface relaxation plays no role. In a truly semi-infinite polar slab, such as the one schematized in figure 2(a), the *macroscopic* component of the dipole moment is entirely determined by the charges and layer spacings in the *bulk* repeat unit. Consequently, a mere contraction or dilation of the interlayer spacings in the vicinity of the surface, not accompanied by a change in the layer charge densities, can never cancel the polarity. This is why the electrostatic condition (2.1) does not depend upon the layer spacings.

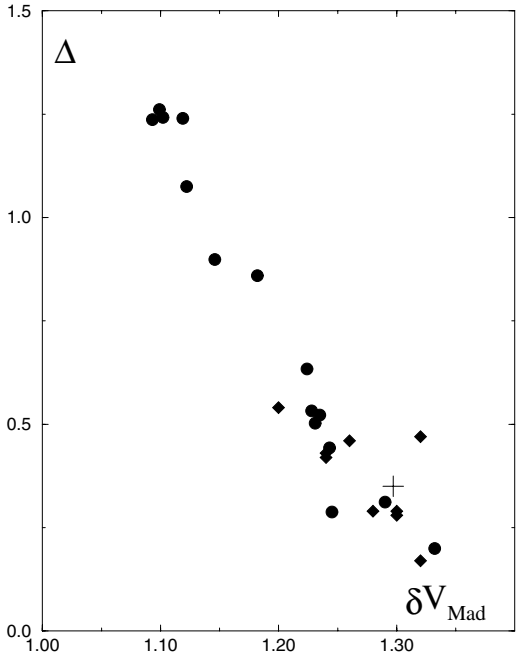

Figure 20. Variations of the Ti–O electron transfer per bond Δ as a function of the changes in $\epsilon_C - \epsilon_A$ associated with the Madelung potential, in small neutral $(TiO_2)_n$ clusters, the $TiO_2(110)$ surface, and bulk rutile TiO_2. Note the large variations of Δ, whose biggest values are associated with bonds which involve highly undercoordinated atoms and whose smallest values are obtained for the most compact structures. From reference [235].

However, once charge compensation is achieved—by whatever mechanism—surface relaxation induces a lowering of surface energy, as it does on non-polar surfaces. The strength of the effect increases as the coordination of the surface atoms gets lower [238]. For example, on the charge-compensated α-Al_2O_3 (0001) surface, terminated with a single Al layer, the surface cations are threefold coordinated, while their bulk counterparts have six first neighbours. A strong inward relaxation takes place, which was predicted by classical pair potential approaches, and observed experimentally, and also confirmed by *ab initio* calculations (see section 3.4.1). Similarly, in the classical simulations of the reconstructed (2×1) NiO(111) surface, the surface energy is lowered by as much as 4.9 J m^{-2} by relaxation effects, a large energy stabilization associated with the very low coordination number of the surface atoms [239].

4.2.2. Change of covalency in the surface layers. Since charge compensation requires a modification of the charge density in the surface layers, it is often thought that a change of covalency at the surface can cancel the polarity. With the help of the bond-transfer model, we will show that this statement is incorrect, as far as semi-infinite polar surfaces are concerned. It will be useful to distinguish between weakly polar surfaces, in which the dipole moment in the repeat unit is entirely due to covalent effects, and truly polar surfaces whose dipole moment contains an integer contribution. As already stated, in the fully ionic limit, the former ones are considered as non-polar, while the latter ones are recognized as polar.

A prototype of the first family is $SrTiO_3(100)$. In the bulk, there are two different electron transfers per bond, Δ_{Ti-O} and Δ_{Sr-O}, associated with the σ-overlap of O orbitals with Ti 3d

orbitals and Sr 5s orbitals, respectively. Taking into account the coordination number of the atoms and assuming a complete filling of the valence band, as we have done in section 4.1.3 for bulk MgO, the electron numbers and charges read

$$\begin{aligned} N_{\mathrm{Ti}} &= 6\Delta_{\mathrm{Ti-O}} & Q_{\mathrm{Ti}} &= 4 - 6\Delta_{\mathrm{Ti-O}} \\ N_{\mathrm{Sr}} &= 12\Delta_{\mathrm{Sr-O}} & Q_{\mathrm{Sr}} &= 2 - 12\Delta_{\mathrm{Sr-O}} \\ N_{\mathrm{O}} &= 8 - 2\Delta_{\mathrm{Ti-O}} - 4\Delta_{\mathrm{Sr-O}} & Q_{\mathrm{O}} &= -2 + 2\Delta_{\mathrm{Ti-O}} + 4\Delta_{\mathrm{Sr-O}} \end{aligned} \tag{4.5}$$

which yields charge densities of $\pm\sigma_{\mathrm{B}}$ per two-dimensional unit cell, on the bulk (100) TiO_2 and SrO layers:

$$\sigma_{\mathrm{B}} = |Q_{\mathrm{Ti}} + 2Q_{\mathrm{O}}| = Q_{\mathrm{Sr}} + Q_{\mathrm{O}} = 2\Delta_{\mathrm{Ti-O}} - 8\Delta_{\mathrm{Sr-O}}. \tag{4.6}$$

The dipole moment in the bulk repeat unit is thus non-zero. However, it has no integer contribution and depends only on covalent effects.

On the (100) surface, due to the change in local environment, due to possible structural distortions and due to shifts of atomic levels, redistributions of charge take place. On the TiO_2 termination, for instance, titaniums are fivefold coordinated (instead of sixfold) and oxygens have lost two strontium neighbours. Modified electron transfers $\Delta'_{\mathrm{Ti-O}}$ and $\Delta'_{\mathrm{Sr-O}}$ have also to be introduced for bonds involving the surface Ti or O (figure 21). This yields atomic charges which differ from the bulk in two layers (layers are indexed by $n \geqslant 1$, starting from the vacuum):

$$\begin{aligned} Q_{\mathrm{Ti}_1} &= 4 - 5\Delta'_{\mathrm{Ti-O}} & Q_{\mathrm{O}_1} &= -2 + 2\Delta'_{\mathrm{Ti-O}} + 2\Delta'_{\mathrm{Sr-O}} \\ Q_{\mathrm{Sr}_2} &= 2 - 4\Delta'_{\mathrm{Sr-O}} - 8\Delta_{\mathrm{Sr-O}} & Q_{\mathrm{O}_2} &= -2 + \Delta'_{\mathrm{Ti-O}} + \Delta_{\mathrm{Ti-O}} + 4\Delta_{\mathrm{Sr-O}} \end{aligned} \tag{4.7}$$

and layer charge densities equal to

$$\begin{aligned} \sigma_1 &= -\Delta'_{\mathrm{Ti-O}} + 4\Delta'_{\mathrm{Sr-O}} \\ \sigma_2 &= \Delta'_{\mathrm{Ti-O}} + \Delta_{\mathrm{Ti-O}} - 4\Delta'_{\mathrm{Sr-O}} - 4\Delta_{\mathrm{Sr-O}} \\ \sigma_{\mathrm{B}} &= -2\Delta_{\mathrm{Ti-O}} + 8\Delta_{\mathrm{Sr-O}}. \end{aligned} \tag{4.8}$$

It is found that $\sigma_1 + \sigma_2 = \Delta_{\mathrm{Ti-O}} - 4\Delta_{\mathrm{Sr-O}}$, which fulfils the condition $\sigma_1 + \sigma_2 = -\sigma_{\mathrm{B}}/2$ (equation (2.1)) whatever the specific values of the Δ and Δ' parameters are. On $SrTiO_3$(100), the bond-breaking mechanism, by itself, thus yields the charge redistribution which suppresses the divergent part of electrostatic potential. The surface charges are different from the bulk ones, both because the bond covalency in the surface layers is different from that in the bulk ($\Delta' \neq \Delta$) and because the coordination of surface atoms is reduced with respect to that of the bulk atoms. However, the model shows that only the second factor is effective for cancelling the polarity, while the change of covalency plays no role in the charge-compensation process.

We now consider the second family of polar surfaces, in which the dipole moment borne by the bulk repeat unit contains an integer contribution. We will show that in this case also, a change in covalency in the surface layers cannot cancel the polarity. MgO(111) will be used as the representative of this family.

Using the charge values already derived for bulk MgO (equation (4.2)), the charge density per (1×1) unit cell on bulk (111) layers is equal to $\sigma_{\mathrm{B}} = \pm(2 - 6\Delta)$. On a stoichiometric (111) magnesium termination, surface atoms are threefold coordinated to atoms located in the underlying layers; the electron transfer Δ' between the surface and sub-surface layer is different from its bulk value Δ (figure 21). If only valence band states were filled, one would obtain the following electron numbers and charges:

$$\begin{aligned} N_{\mathrm{Mg}_1} &= 3\Delta' & Q_{\mathrm{Mg}_1} &= 2 - 3\Delta' \\ N_{\mathrm{O}_2} &= 8 - 3\Delta' - 3\Delta & Q_{\mathrm{O}_2} &= -2 + 3\Delta' + 3\Delta \\ N_{\mathrm{B}} &= 6\Delta & Q_{\mathrm{B}} &= 2 - 6\Delta. \end{aligned} \tag{4.9}$$

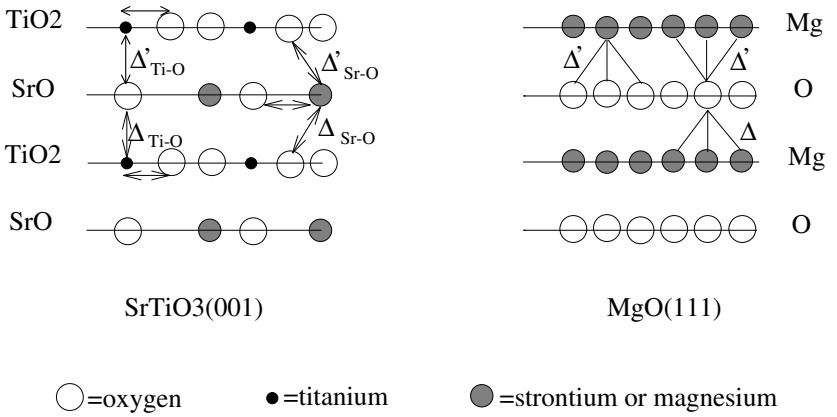

Figure 21. Electron transfers per bond introduced in the modellization of an $SrTiO_3(001)$ surface (left panel) and of a MgO(111) surface (right panel). On $SrTiO_3(001)$, specific transfers Δ'_{Ti-O} and Δ'_{Sr-O} (represented by thick arrows) are introduced inside the surface layer and in between the surface and sub-surface layers for Ti–O bonds and Sr–O bonds involving surface atoms. On MgO(111), only the first interplane transfer is assumed to be modified.

This equation tells us that the charges borne by the atoms in the outermost layer ($n = 1$) are different from those borne by atoms in the bulk. But the same is also true for atoms in the sub-surface layer ($n = 2$) because $\Delta' \neq \Delta$. Q_{Mg_1} and Q_{O_2} are such that $\sigma_1 + \sigma_2 = 3\Delta$. This does not fulfil the electrostatic criterion, which, instead, requires that $\sigma_1 + \sigma_2 = 3\Delta - 1$. The surface layers have a deficit of one electron, which is independent of the values of Δ' and Δ. It should be noted that the same result is obtained in a fully ionic picture ($\Delta' = \Delta = 0$) or when neglecting the change of covalency ($\Delta' = \Delta$). In this family also, thus, charge compensation cannot be achieved by change of covalency at the surface.

What we have demonstrated in this section is very general: a mere change of covalency in the outer layer can never provide the compensating charges, because it concerns several layers whose contributions cancel out in the expression of the electrostatic criterion.

4.2.3. Filling of surface states. On stoichiometric polar surfaces, charge compensation can only be achieved by a partial/total filling of conduction band surface states or depletion of valence band surface states. The bond-transfer model helps with understanding that this filling can be determined by ionic arguments, even for very covalent materials, and that it is not related to the specificities of hybridization in the outer layers. We exemplify this point for MgO(111).

On the MgO(111)–Mg termination, since one electron per unit cell is missing to fulfil equation (2.1) when only the valence band is filled, we now consider the possibility of additionally filling a conduction band state. Madelung potential arguments tell us that the lowest-energy conduction band state is derived from orbitals of magnesiums located in the outermost layer. Assuming an occupation factor f for this state (per surface unit cell), the electron counting becomes (with the same notation as in section 4.2.2)

$$\begin{aligned} N_{Mg_1} &= 2f + 3\Delta' - 3f\delta & Q_{Mg_1} &= 2(1-f) - 3\Delta' + 3f\delta \\ N_{O_2} &= 8 - 3\Delta' - 3\Delta + 3f\delta & Q_{O_2} &= -2 + 3\Delta' + 3\Delta - 3f\delta \\ N_B &= 6\Delta & Q_B &= 2 - 6\Delta \end{aligned} \tag{4.10}$$

which yields $\sigma_1 + \sigma_2 = -2f + 3\Delta$. Charge compensation is thus achieved if $f = 1/2$. The analysis of the oxygen termination leads to the symmetric conclusion that a surface valence

band state has to be half-filled. It should be noted that the condition $f = 1/2$ is independent of the precise values of the electron transfers per bond Δ', Δ, and δ. The conclusion reached would have been similar using a fully ionic picture.

The result that we have obtained is not restricted to ionic oxides such as MgO. On ZnO(0001) or $SrTiO_3$(111) or (110), the occupancy of surface states is also dictated by the values of the formal charges and of the interlayer spacings R_1 and R_2, despite the fact that these are rather covalent oxides.

The ionic limit can thus be currently used to estimate the value of f required for charge compensation. Two cases occur. In the first case, f is non-integer. The surface states are only partly filled or empty and the surface layers have a 'metallic' character†. This occurs on the rock-salt oxide (111) surfaces ($f = 1/2$), the ZnO(0001) surface ($f = 1/4$), the oxygen termination of the corundum oxide (0001) surface ($f = 1.5$), etc. These partial fillings were indeed found in the quantum calculations quoted in section 3. For some other polar surfaces, f is integer. f surface states are thus filled or empty and the surface can remain insulating. This takes place, for example, on the (111) or (110) polar surfaces of $SrTiO_3$ ($f = 1$).

4.2.4. Change of stoichiometry. Charge compensation can also be achieved by changing the atomic density in the outer layers. The bond-transfer model helps with understanding that the required modifications of stoichiometry are entirely determined by ionic arguments, and not by the specificities of hybridization in the outer layers. We illustrate this point again in the case of MgO(111), and restrict ourselves to modifications of the composition in the outermost layer, chosen to be cationic. We consider a two-dimensional supercell containing M surface Mg atoms, from which we remove one atom. Our goal is to determine, as a function of M, the filling of surface states consistent with charge compensation.

Under these conditions, the surface layer ($n = 1$) contains $M - 1$ threefold-coordinated magnesiums, and the subsurface layer ($n = 2$), $M - 3$ sixfold-coordinated oxygens (charge Q_{O_2}) and three fivefold-coordinated oxygens (charge Q'_{O_2}) (figure 22). The atoms in the layer below are bulk-like. We assume that the valence band states are filled and a conduction band state is partially occupied. Whether the latter is localized on a single magnesium or shared between all equivalent surface atoms, the same layer charge densities are yielded. The equations below are written under the second assumption. We also introduce an electron transfer $\Delta' \neq \Delta$ when surface atoms are involved and a transfer δ related to the conduction band state. The charges on the different atoms are the following:

$$\begin{aligned} Q_{Mg_1} &= 2(1-f) - 3\Delta' + 3f\delta \\ Q_{O_2} &= -2 + 3\Delta' + 3\Delta - 3f\delta \\ Q'_{O_2} &= -2 + 2\Delta' + 3\Delta - 2f\delta \\ Q_B &= 2 - 6\Delta \end{aligned} \tag{4.11}$$

which yields the following charge densities per supercell:

$$\begin{aligned} \sigma_1 &= (M-1)Q_{Mg_1} = (M-1)\left[2(1-f) - 3\Delta' + 3f\delta\right] \\ \sigma_2 &= (M-3)Q_{O_2} + 3Q'_{O_2} = M(-2+3\Delta) + 3\Delta'(M-1) - 3f\delta(M-1) \\ \sigma_B &= MQ_B = M(2-6\Delta). \end{aligned} \tag{4.12}$$

† We use here the term 'metallic' for the sake of simplicity, meaning that electronic excitations of zero energy can be produced. However, when the Fermi level crosses a narrow band, as occurs on the oxygen termination of MgO(111) for example, and when the surface metallization would survive in the limit of zero bandwidth (no electron delocalization, zero value of the resonance integrals), the system should rather be called an 'open-shell' system.

Since $\sigma_1 + \sigma_2 = -2 - 2f(M-1) + 3M\Delta$, the electrostatic criterion $\sigma_1 + \sigma_2 = -\sigma_B$ requires that

$$f = \frac{1}{2}\frac{(M-2)}{(M-1)}. \tag{4.13}$$

Once again, this relationship is independent of the values of the electron transfers per bond. The simplest achievement of this relationship, with no filled conduction band ($f = 0$), is obtained for $M = 2$. This amounts to removing half of the surface atoms from the outermost layer. A similar reasoning, assuming modifications of stoichiometry in two surface layers instead of one, would lead to the octopolar surface configuration.

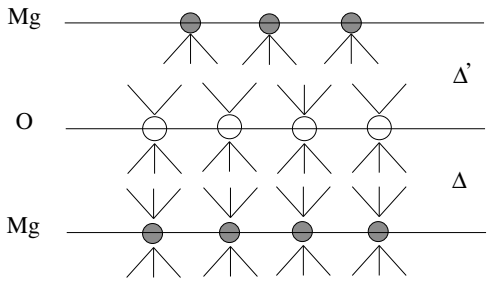

MgO(111)

Figure 22. A schematic representation of a MgO(111) supercell containing $M = 4$ atoms, from which one atom has been removed in the outer layer. The three surface magnesiums are threefold coordinated. Among the four underlying oxygens, three are fivefold coordinated and one is sixfold coordinated.

To summarize, it is possible to predict which stoichiometry, in the surface layers, compatible with an insulating band structure, yields charge compensation, only on the basis of ionic considerations, even for very covalent compounds. This does not mean that covalency effects are absent, or that they are the same as in the bulk, but rather that they cancel out in equation (2.1), which gives the criterion for charge compensation. Charge-compensated non-stoichiometric surfaces, such as the (2×2) octopolar reconstructed rock-salt (111) surfaces, have electronic properties which present no anomaly. However, due to the presence of surface atoms with low coordination numbers, interesting phenomena for applications, such as a reduction of the gap, an increase in basicity of surface oxygens, or an increase in acidity of surface metal atoms can be expected, as on open non-polar surfaces [236, 237, 240, 241].

4.2.5. Specificities of ultrathin films. In this section, we wish to address several questions related to polarity in ultrathin films. As described in section 3, experimentalists have gained an expertise in controlling film thicknesses with a precision better than a monolayer, which has led to the fabrication and characterization of ultrathin films made of just a few monolayers only. It is thus of interest to reconsider the concepts established for semi-infinite systems to understand up to which point they are still valid. However, due to the recent development of research in this field, only qualitative statements regarding surface stability can be extracted from the literature. I try to summarize them in this section. The first point discusses the validity of the electrostatic concepts given in section 2, when the film thickness becomes of the order of one repeat unit. The second point is related to the existence of precise boundary conditions at the interface with the substrate, and the third one concerns the relative stability of symmetric versus non-symmetric films.

The electrostatic criterion for surface stability, equation (2.1), relies on the cancellation of the *macroscopic* dipole moment, i.e. the contribution which increases with thickness. *Stricto sensu*, it only applies to semi-infinite systems in which all the repeat units are bulk-like, except for a few ones in the vicinity of the surfaces. For this reason, equation (2.1) involves only bulk quantities (charges and interlayer spacings). However, in ultrathin films, such as the FeO(111) bilayer grown on a platinum substrate (section 3.2.4), it seems clear that polarity may be cancelled by other means than those discussed previously. Decreasing the spacing between the Fe and O layers, for example, may be efficient, because it reduces both the length of the total dipole and the charges borne by the atoms, through an increase of covalency. The observed large surface relaxation of the FeO bilayer is probably the reason for the existence of a stoichiometric unreconstructed film. Another process, involving a layer exchange, was proposed in the simulation of Fe_3O_4(111) thin films [104]. It is currently not clear how the monolayer limit is connected to the semi-infinite macroscopic limit, and whether there exists a critical thickness above which macroscopic arguments apply again. If so, very probably, this critical thickness has to be very small, due to the rapid increase (more than 10 V per repeat unit) of electrostatic potentials in polar films.

In the case of film orientations which possess non-polar as well as polar terminations, such as the corundum (0001) orientation, the boundary conditions at the interface with the substrate may play a role of prime importance in the surface stability, which is, however, rarely referred to. For example, a configuration which starts from the substrate (S) as $S/M/O_3/M/M/O_3/M/\cdots$ (figures 23(a) and 23(b)) will probably exhibit any of the three possible terminations, because the 'bulk' repeat unit has no dipole moment, and because the film grows through the deposition of *neutral* atoms. The oxygen termination, in particular, will be associated with a *surface* dipole moment, but not with a *macroscopic* dipole moment (figure 23(b)). Its surface energy is thus expected to be relatively low. On the other hand, if the film grows on the substrate with the following sequence: $S/O_3/M/M/O_3/M/\cdots$ (figures 23(c) and 23(d)) or $S/M/M/O_3/M/M/O_3/M/\cdots$, then only the $M/O_3/M$ termination in contact with the vacuum will be stable (figure 23(c)). This is because repeat units starting from the vacuum will have zero dipole moments. Only at the interface will there be a non-zero polarization, possibly smoothed by charge transfer from or to the substrate. This will not give rise to polarity effects, unlike the cases for the $O_3/M/M$ or $M/M/O_3$ terminations (figure 23(d)).

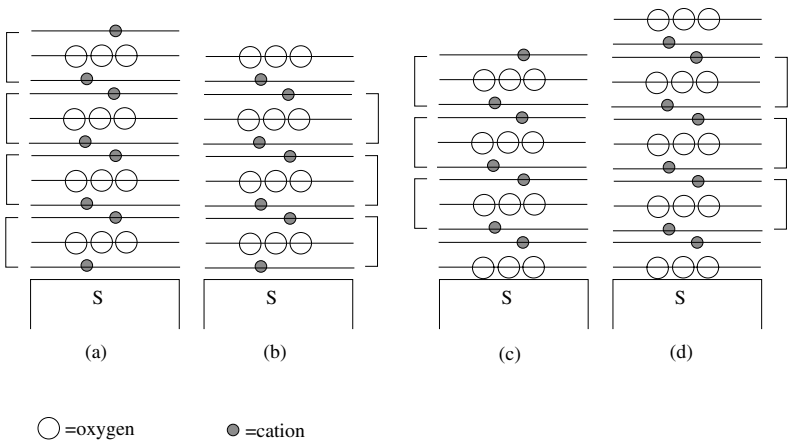

Figure 23. Schematic profile views of a corundum (0001) thin film grown on a substrate S, assuming different sequences of growth. Note the absence of a *macroscopic* dipole moment in the (a), (b), and (c) configurations.

A final remark concerns the widespread belief that a symmetric slab is more stable than a non-symmetric one, because it contains no net dipole moment. This can be exemplified by comparing the energetics and the electronic structure of Mg/O/···/Mg/O/Mg and Mg/O/···/Mg/O (111) films. First, since symmetric and non-symmetric slabs do not have the same stoichiometry, their relative stability cannot be estimated via their internal energy, but rather has to be estimated via their Gibbs free energy, which is a function of the partial pressure of oxygen, for example. Moreover, the distortions of the electronic structure which take place on the outer layers of both slabs are very similar, despite the fact that no macroscopic dipole moment exists in the symmetric slab. We have checked this point numerically in the case of MgO(111) [36]. It can also be proved with the help of the bond-transfer model or with the following simple argument. Let us start with a non-symmetric slab Mg/O/···/Mg/O and let us consider its O termination. If the outer layer is stoichiometric, an oxygen-derived surface state is half-filled. Depositing one neutral Mg layer on top provides two electrons per surface unit cell: one of them completes the filling of the pre-existing oxygen-derived surface state and the other partly fills a Mg-derived state in the new surface conduction band. This yields a Mg termination similar to that on the other side of the slab. This result is an important one, both with respect to the understanding of polar thin films and because it proves that the slab model for representing semi-infinite systems is not biased by spurious interactions between the two terminations.

4.3. Summary

Polar oxide surfaces present a wide variety of electronic and atomic characteristics, which are dependent upon the crystal structure, the ionicity of the metal–oxygen bonding, and the surface orientation and its stoichiometry. The nature of the microscopic processes responsible for the cancellation of polarity provides a means to introduce a classification among these surfaces.

Weakly polar surfaces are met each time that the dipole moment in the repeat unit is a function of the electron transfers per bond only and does not involve integer contributions, as in the case of $SrTiO_3$(100). On stoichiometric surfaces, the charge compensation may be attributed to the effect of bond breaking. The surface LDOS differs from the bulk one because of the reduced local environment of the surface atoms (different effective atomic orbital energies, bond-length modifications, change in the coordination numbers). However, the terminations are insulating, with filled oxygen-derived surface states and empty metal-derived surface states. These surfaces have low surface energies and can be produced stoichiometric and planar. We have called them previously *weakly polar surfaces*, because their polar instability is weak.

For fully polar surfaces, the surface dipole in the repeat unit contains an integer contribution, independently of the values of the electron transfer per bond. For semi-infinite surfaces, it was shown that a mere change of covalency in the outer layers can never provide the compensating charges, because it modifies the charges of several types of atom whose contributions cancel out in the expression for the electrostatic criterion. Similarly, and for the same reason, surface relaxation cannot provide the compensating charges. Only a modification in the filling of surface states or a change in the stoichiometry of the surface layers may yield charge compensation.

It turns out that if stoichiometric polar surfaces are unstable, this is never because they present a diverging electrostatic surface energy. The compounds have enough degrees of freedom, and in particular enough flexibility of their electronic structure in response to the surface potential, to cancel the polarity while remaining stoichiometric. If a partial filling

of surface states is required—and, as shown above, this can be estimated assuming a fully ionic limit—as in the rock-salt (111), wurtzite (0001) or $(000\bar{1})$, etc, surfaces, the terminations present a 'metallic' character. This is usually not favourable, from an energetic point of view, as recognized in the expression of the auto-compensation principle.

On other stoichiometric polar surfaces, an integer filling of surface states is required. This is the case on $SrTiO_3$ or $BaTiO_3$(110) and (111) surfaces. The surfaces thus may remain insulating but a conduction state is located below E_F. Self-consistent calculations give a hint that this electronic structure is not associated with a high surface energy. They support preliminary experimental observations of non-reconstructed perovskite (111) and (110) surfaces. This suggests that the auto-compensation principle (filled anion-derived surface states and empty cation-derived surface states) should be extended to include all insulating surface configurations, whatever the nature of the filled and empty states. However, for perovskite compounds, the absence of reconstruction is not necessarily equivalent to stoichiometry being achieved, and further work should assess this point in the future, by determining quantitatively surface compositions.

Polarity may also be cancelled by the removal of a certain percentage of atoms in the outer layers. When the vacancies order, most of the time, this leads to surface reconstructions. We have seen that the surface concentrations compatible with a vanishing macroscopic dipole moment can be correctly estimated within a fully ionic picture. Low-energy configurations are expected to be insulating, and indeed, on non-polar oxide surfaces, a correlation has been found between the stability of a surface orientation and the surface gap value [236, 237].

Finally, ultrathin polar films present specificities due to the absence of 'bulk' layers, below a critical thickness. Modification of covalency, surface relaxation, as well as diffusion of atoms in the film are possible processes for decreasing the electrostatic energy, but their efficiency is not currently quantitatively assessed.

5. Conclusions

We have summarized our present understanding of polar oxide surfaces. It appears that, compared to semiconductor compound surfaces, they present more diversity, as regards their crystallographic structures, their anion–cation bonding, and their magnetic properties. The possible existence of mixed-valence compounds, and of several oxide stoichiometries for a given metal atom, makes this field fascinating on fundamental grounds and rich in possible applications.

We have shown that, in the case of semi-infinite materials, and at least for simple charge-transfer oxides, it is possible to rationalize different scenarios for the cancellation of polarity and assess the efficiency of several processes which have been referred to in the literature, such as the change of covalency in the surface layers, the surface relaxation, the filling of surface states, and the non-stoichiometry. It is clear that much work remains to be done to extend our understanding to transition metal oxides with d^n configurations. On the experimental side, it seems that one of the present bottlenecks is in a quantitative determination of the surface stoichiometry, information of prominent interest as regards interpreting the presence or absence of reconstruction.

Advances in the control of ultrathin layers, allowing the stabilization of orientations which are not accessible when cutting a bulk material, open the way to the fabrication of artificial structures for controlled catalysis or of nano-structured substrates for electronic or magnetic applications.

Acknowledgments

Discussions with F Finocchi, J Goniakowski, H J Freund, W Weiss, W C Mackrodt, H Neddermeyer and M Gautier-Soyer are gratefully acknowledged. I thank A Barbier, N Jedrecy and M Sauvage-Simkin for communication of their results prior to publication.

References

[1] Noguera C 1996 *Physics and Chemistry at Oxide Surfaces* (Cambridge: Cambridge University Press)
[2] Kahn A 1996 *Surf. Rev. Lett.* **3** 1579
[3] Henrich V E and Cox P A 1994 *The Surface Science of Metal Oxides* (Cambridge: Cambridge University Press)
[4] Kuhlenbeck H and Freund H J 1997 *Growth and Properties of Ultrathin Epitaxial Layers (The Chemical Physics of Solid Surfaces, vol 8)* ed D A King and D P Woodruff (Amsterdam: Elsevier) ch 9, p 340
[5] Tasker P W 1979 *J. Phys. C: Solid State Phys.* **12** 4977
[6] Nosker R W, Mark P and Levine J D 1970 *Surf. Sci.* **19** 291
[7] Vanderbilt D and King-Smith R D 1993 *Phys. Rev.* B **48** 4442
[8] Kuntzinger S, Ghermani N E, Dusausoy Y and Lecomte C 1998 *Acta Crystallogr.* B **54** 819
[9] See e.g. Parr R G and Wang Y 1989 *Density Functional Theory of Atoms and Molecules* (Oxford: Oxford University Press)
[10] Noguera C, Pojani A, Finocchi F and Goniakowski J 1997 *Chemisorption and Reactivity on Supported Clusters and Thin Films: Towards an Understanding of Microscopic Processes in Catalysis (NATO ASI Series E: Applied Sciences, vol 331)* ed R M Lambert and G Pacchioni (Dordrecht: Kluwer) p 455
[11] Duke C B 1996 *Chem. Rev.* **96** 1237
[12] Renaud G 1998 *Surf. Sci. Rep.* **32** 1
[13] Kaxiras E, Bar-Yam Y and Joannopoulos J D 1987 *Phys. Rev.* B **35** 9625
[14] Shiraishi K 1990 *J. Phys. Soc. Japan* **59** 3455
[15] Yamauchi J, Tsukada M, Watanabe S and Sugino O 1996 *Phys. Rev.* B **54** 5586
[16] Mankefors S 1999 *Phys. Rev.* B **59** 13 151
[17] Phillips J C 1970 *Rev. Mod. Phys.* **42** 317
[18] Wolf D 1992 *Phys. Rev. Lett.* **68** 3315
[19] Barbier A and Renaud G 1997 *Surf. Sci. Lett.* **392** L15
[20] Barbier A, Renaud G, Mocuta C and Stierle A 1999 *Surf. Sci.* **433–435** 761
[21] Warren O L and Thiel P A 1994 *J. Chem. Phys.* **100** 659
[22] Rohr F, Wirth K, Libuda J, Cappus D, Baümer M and Freund H J 1994 *Surf. Sci.* **315** L977
[23] Cappus D, Xu C, Ehrlich D, Dillmann B, Ventrice C A Jr, Al-Shamery K, Kuhlenbeck H and Freund H J 1993 *Chem. Phys.* **177** 533
[24] Hannemann H, Ventrice C A Jr, Bertrams T, Brodde A and Neddermeyer H 1994 *Phys. Status Solidi* a **146** 289
[25] Ventrice C A Jr, Bertrams T, Hannemann H, Brodde A and Neddermeyer H 1994 *Phys. Rev.* B **49** 5773
[26] Oliver P M, Watson G W and Parker S C 1995 *Phys. Rev.* B **52** 5323
[27] Barbier A, Mocuta C, Kuhlenbeck H, Peters K F, Richter B and Renaud G 2000 *Phys. Rev. Lett.* **84** 2897
[28] Mocuta C, Barbier A, Renaud G and Dieny B 1998 *Thin Solid Films* **336** 160
[29] Barbier A, Renaud G, Mocuta C and Stierle A 1999 *Proc. IWOX1 Conf. (Elmau, Germany)*
[30] Henrich V E 1976 *Surf. Sci.* **57** 385
[31] Onishi H, Egawa C, Aruga T and Iwasawa Y 1987 *Surf. Sci.* **191** 479
[32] Plass R, Feller J and Gajdardziska-Josifovska M 1998 *Surf. Sci.* **414** 26
[33] Plass R, Egan K, Collazo-Davila C, Grozea D, Landree E, Marks D L and Gajdardziska-Josifovska M 1998 *Phys. Rev. Lett.* **81** 4891
[34] Henry C R and Poppa H 1990 *Thin Solid Films* **189** 303
[35] Tsukada M and Hoshino T 1982 *J. Phys. Soc. Japan* **51** 2562
[36] Pojani A, Finocchi F, Goniakowski J and Noguera C 1997 *Surf. Sci.* **387** 354
[37] Goniakowski J and Noguera C 1999 *Phys. Rev.* B **60** 16 120
[38] Watson G W 1996 *J. Chem. Soc. Faraday Trans.* II **92** 433
[39] Baudin M, Wojcik M and Hermansson K 1997 *Surf. Sci.* **375** 374
[40] Hermansson K, Baudin M, Ensing B, Alfredsson M and Wojcik M 1998 *J. Chem. Phys.* **109** 7515
[41] Parker S C, de Leeuw N H and Redfern S E 1999 *Discuss. Faraday Soc.* **114** 381
[42] Refson K, Wogelius R A, Fraser D G, Payne M C, Lee M H and Milman V 1995 *Phys. Rev.* B **52** 10 823

[43] He J W and Møller P J 1986 *Surf. Sci.* **178** 934
[44] Mattsson J E, Fullerton E E, Sowers C H and Bader S D 1995 *J. Vac. Sci. Technol.* A **13** 276
[45] Fornander H, Dannetun H and Ekedahl L G 1999 *Surf. Sci.* **440** 375
[46] Sandström P, Svedberg E B, Birch J and Sundgren J E 1999 *Surf. Sci. Lett.* **437** L767
[47] Lu P and Cosandey F 1992 *Ultramicroscopy* **40** 271
[48] Lu P and Cosandey F 1992 *Acta Metall. Mater.* **40** S259 (supplement)
[49] Chen F R, Chiou S K, Chang L and Hong C S 1994 *Ultramicroscopy* **54** 179
[50] Shashkov D A and Seidman D N 1995 *Phys. Rev. Lett.* **75** 268
[51] Imhoff D, Laurent S, Colliex C and Backhaus-Ricoult M 1999 *Eur. Phys. J. Appl. Phys.* **5** 9
[52] Backhaus-Ricoult M 1999 *Proc. Int. Conf. on Interfaces (Seville)*
[53] Benedek R, Minkoff M and Yang L H 1996 *Phys. Rev.* B **54** 7697
[54] Benedek R, Seidman D N, Minkoff M, Yang L H and Alavi A 1999 *Phys. Rev.* B **60** 16 094
[55] Muller D A, Shashkov D A, Benedek R, Yang L H, Silcox J and Seidman D N 1998 *Phys. Rev. Lett.* **80** 4741
[56] Bridge M E and Lambert R M 1979 *Surf. Sci.* **82** 413
[57] Bardi U, Beard B C and Ross P N 1988 *J. Vac. Sci. Technol.* A **6** 665
[58] Hassel M and Freund H J 1995 *Surf. Sci.* **325** 163
[59] Hassel M and Freund H J 1996 *Surf. Sci. Spectra* **4** 273
[60] Schonnenbeck M, Cappus D, Klinkmann J, Freund H J, Petterson L G M and Bagus P S 1996 *Surf. Sci.* **347** 337
[61] Sebastian I, Heiler M, Meinel K and Neddermeyer H 1998 *Appl. Phys.* A **66** S525
[62] Mocuta C, Barbier A and Renaud G 2000 *Appl. Surf. Sci.* at press
[63] Cappus D, Hassel M, Neuhaus E, Heber M, Rohr F and Freund H J 1995 *Surf. Sci.* **337** 268
[64] Vurens G H, Maurice V, Salmeron M and Somorjai G A 1992 *Surf. Sci.* **268** 170
[65] Galloway H C, Benitez J J and Salmeron M 1993 *Surf. Sci.* **298** 127
[66] Galloway H C, Benitez J J and Salmeron M 1994 *J. Vac. Sci. Technol.* A **12** 2302
[67] Schedel-Niedrig T, Weiss W and Schlögl R 1995 *Phys. Rev.* **52** 17 449
[68] Ritter M, Over H and Weiss W 1997 *Surf. Sci.* **371** 245
[69] Weiss W 1997 *Surf. Sci.* **377–379** 943
[70] Ritter M, Ranke W and Weiss W 1998 *Phys. Rev.* B **57** 7240
[71] Corneille J S, He J W and Goodman D W 1995 *Surf. Sci.* **338** 211
[72] Maeda T, Kobayashi Y and Kishi K 1999 *Surf. Sci.* **436** 249
[73] Gota S, Guiot E, Henriot M and Gautier-Soyer M 1999 *Phys. Rev.* B **60** 14 387
[74] Koike K and Furukawa T 1996 *Phys. Rev. Lett.* **77** 3921
[75] Ranke W, Ritter M and Weiss W 1999 *Phys. Rev.* B **60** 1527
[76] Kim Y J, Westphal C, Ynzunza R X, Galloway H C, Salmeron M, Van Hove M A and Fadley C S 1997 *Phys. Rev.* B **55** R13 448
[77] Galloway H C, Sautet P and Salmeron M 1996 *Phys. Rev.* B **54** R11 145
[78] Ranke W and Weiss W 1998 *Surf. Sci.* **414** 236
[79] Zscherpel D, Ranke W, Weiss W and Schlögl R 1998 *J. Chem. Phys.* **108** 1
[80] Joseph Y, Kuhrs C, Ranke W and Weiss W 1999 *Surf. Sci.* **435** 114
[81] Shvets I V, Wiesendanger R, Burgler D, Tarrach G, Guntherodt H J and Coey J M D 1992 *J. Appl. Phys.* **71** 5489
[82] Wiesendanger R, Shvets I V, Burgler D, Tarrach G, Guntherodt H J and Coey J M D 1992 *Europhys. Lett.* **19** 141
[83] Tarrach G, Burgler D, Schaub T, Wiesendanger R and Guntherodt H J 1993 *Surf. Sci.* **285** 1
[84] Wiesendanger R, Shvets I V and Coey J M D 1994 *J. Vac. Sci. Technol.* B **12** 2118
[85] Fujii T, Takano M, Katano R, Bando Y and Isozumi Y 1990 *J. Cryst. Growth* **99** 606
[86] van der Heijden P A A, Bloemen P J H, Gaines J M, van Eemeren J T W M, Wolf R M, van der Zaag P J and de Jonge W J M 1996 *J. Magn. Magn. Mater.* **159** L293
[87] Fontijn W F J, Wolf R M, Metselaar R and van der Zaag P J 1997 *Thin Solid Films* **292** 270
[88] Gaines J M, Bloemen P J H, Kohlhepp J T, Bulle Lieuwma C W T, Wolf R M, Reinders A, Jungblut R M, van der Heijden P A A, van Eemeren J T W M, Aan de Stegge J and de Jonge W J M 1997 *Surf. Sci.* **373** 85
[89] Kim Y J, Gao Y and Chambers S A 1997 *Surf. Sci.* **371** 358
[90] Gao Y and Chambers S A 1997 *J. Cryst. Growth* **174** 446
[91] Chambers S A and Joyce S A 1999 *Surf. Sci.* **420** 111
[92] Fujii T, de Groot F M F, Sawatzky G A, Voogt F C, Hibma T and Okada K 1999 *Phys. Rev.* B **59** 3195
[93] Voogt F C, Fujii T, Smulders P J M, Niesen L, James M A and Hibma T 1999 *Phys. Rev.* B **60** 11 193
[94] Weiss W, Barbieri A, Van Hove M A and Somorjai G A 1993 *Phys. Rev. Lett.* **71** 1848

[95] Barbieri A, Weiss W, Van Hove M A and Somorjai G A 1994 *Surf. Sci.* **302** 259
[96] Ritter M and Weiss W 1999 *Surf. Sci.* **432** 81
[97] Lad R J and Henrich V E 1989 *Phys. Rev.* B **39** 13 478
[98] Cai Y Q, Ritter M, Weiss W and Bradshaw A M 1998 *Phys. Rev.* B **58** 5043
[99] Shaikhutdinov Sh K, Ritter M, Wang X G, Over H and Weiss W 1999 *Phys. Rev.* B **60** 11 062
[100] Condon N G, Murray P W, Leibsle F M, Thornton G, Lennie A R and Vaughan D J 1994 *Surf. Sci.* **310** L609
[101] Fujii T, Takano M, Katano R, Bando Y and Isozumi Y 1990 *J. Appl. Phys.* **68** 1735
[102] Gao Y, Kim Y J, Bai G and Chambers S A 1997 *J. Vac. Sci. Technol.* A **15** 332
[103] Lennie A R, Condon N G, Leibsle F M, Murray P W, Thornton G and Vaughan D J 1996 *Phys. Rev.* B **53** 10 244
[104] Ahdjoudj J, Martinsky C, Minot C, Van Hove M A and Somorjai G A 1999 *Surf. Sci.* **443** 133
[105] French T M and Somorjai G A 1970 *J. Phys. Chem.* **74** 2489
[106] Gautier M, Pham Van L, Guittet M J and Duraud J P 1991 *Surf. Sci.* **250** 71
[107] Gautier M, Renaud G, Pham Van L, Villette B, Pollak M, Thromat N, Jollet F and Duraud J P 1994 *J. Am. Ceram. Soc.* **77** 323
[108] Mackrodt W C, Davey R J, Black S N and Docherty R 1987 *J. Cryst. Growth* **80** 441
[109] Causa M, Pisani C and Roetti C 1989 *Surf. Sci.* **215** 259
[110] Guo J, Ellis D E and Lam D J 1992 *Phys. Rev.* B **45** 13 647
[111] Mackrodt W C 1992 *Phil. Trans. R. Soc.* A **341** 301
[112] Manassidis I and Gillan M J 1994 *J. Am. Ceram. Soc.* **77** 335
[113] Manassidis I and Gillan M J 1994 *Surf. Sci.* **285** L517
[114] Godin T J and LaFemina J P 1994 *Phys. Rev.* B **49** 7691
[115] Puchin V E, Gale J D, Schluger A L, Kotomin E A, Günster J, Brause M and Kempter V 1997 *Surf. Sci.* **370** 190
[116] Verdozzi C, Jennison D R, Schultz P A and Sears M P 1999 *Phys. Rev. Lett.* **82** 799
[117] Guenard P, Renaud G, Barbier A and Gautier-Soyer M 1996 *Mater. Res. Soc. Symp. Proc.* **437** 15
[118] Guenard P, Renaud G, Barbier A and Gautier-Soyer M 1998 *Surf. Rev. Lett.* **5** 321
[119] Ahn J and Rabelais J W 1997 *Surf. Sci.* **388** 121
[120] Renaud G, Villette B, Vilfan I and Bourret A 1994 *Phys. Rev. Lett.* **73** 1825
[121] Gautier-Soyer M, Jollet F and Noguera C 1996 *Surf. Sci.* **352–354** 755
[122] Jaeger R M, Kuhlenbeck H, Freund H J, Wuttig M, Hoffmann W, Franchy R and Ibach H 1991 *Surf. Sci.* **259** 235
[123] Libuda J, Winkelmann F, Baumer M, Freund H J, Bertrams T, Neddermeyer H and Muller K 1994 *Surf. Sci.* **318** 61
[124] Becker C, Kandler J, Raaf H, Linke R, Pelster T, Drager M, Tanemura M and Wandelt K 1998 *J. Sci. Vac. Technol.* A **16** 1000
[125] Chen P J and Goodman D W 1994 *Surf. Sci.* **312** L767
[126] Wu M C and Goodman D W 1994 *J. Phys. Chem.* **98** 9874
[127] Wu Y T, Garfunkel E and Madey T E 1996 *J. Vac. Sci. Technol.* A **14** 2554
[128] Wu Y T, Garfunkel E and Madey T E 1996 *Surf. Sci.* **365** 337
[129] Jennison D R, Verdozzi C, Schultz P A and Sears M P 1999 *Phys. Rev.* B **59** R15 605
[130] Bursill L A and Peng J L 1989 *Phil. Mag.* A **60** 307
[131] Xu C, Dillmann B, Kuhlenbeck H and Freund H J 1991 *Phys. Rev. Lett.* **67** 3551
[132] Xu C, Hassel M, Kuhlenbeck H and Freund H J 1991 *Surf. Sci.* **258** 23
[133] Stierle A and Zabel H 1997 *Surf. Sci.* **385** 167
[134] Stierle A, Koll Th and Zabel H 1998 *Phys. Rev.* B **58** 5062
[135] Zhang L, Kuhn M and Diebold U 1997 *Surf. Sci.* **375** 1
[136] Bender M, Ehrlich D, Yakovkin I N, Rohr F, Baumer M, Kuhlenbeck H, Freund H J and Staemmler V 1995 *J. Phys.: Condens. Matter* **7** 5289
[137] Rohr F, Baumer M, Freund H J, Mejias J A, Staemmler V, Muller S, Hammer L and Heinz K 1997 *Surf. Sci.* **372** L291
[138] Mejias J A, Staemmler V and Freund H J 1999 *J. Phys.: Condens. Matter* **11** 7881
[139] Robberts P S, Geisler H, Ventrice C A, van Ek J, Chaturvedi S, Rodriguez J A, Kuhn M and Diebold U 1998 *J. Vac. Sci. Technol.* A **16** 990
[140] Gloege T, Meyerheim H L, Moritz W and Wolf D 1999 *Surf. Sci.* **441** L917
[141] Cappus D, Xu C, Ehrlich D, Dillmann B, Ventrice C A Jr, Al-Shamery K, Kuhlenbeck H and Freund H J 1993 *Chem. Phys.* **177** 533
[142] Rehbein C, Harrison N M and Wander A 1996 *Phys. Rev.* B **54** 14 066

[143] Bredow T 1998 *Surf. Sci.* **401** 82
[144] San-Miguel M A, Alvarez L J, Sanz J F and Odriozola J A 1999 *J. Mol. Struct. Theochem* **463** 185
[145] Lewis K B, Oyama S T and Somorjai G A 1990 *Surf. Sci.* **233** 75
[146] Kishi K, Hirai K and Yamamoto T 1993 *Surf. Sci.* **290** 309
[147] Zhang Z and Henrich V E 1992 *Surf. Sci.* **277** 263
[148] Guo Q, Lee S and Goodman D W 1999 *Surf. Sci.* **437** 38
[149] Biener J, Baumer M and Madix R J 1999 *Surf. Sci.* **432** 178
[150] Schuler H, Klimm S, Weissmann G, Renner C and Horn S 1997 *Thin Solid Films* **299** 119
[151] Guo Q, Kim D Y, Street S C and Goodman D W 1999 *J. Vac. Sci. Technol.* A **17** 1887
[152] Biener J, Baumer M, Madix R J, Liu P, Nelson E J, Kendelewicz T and Brown G E 1999 *Surf. Sci.* **441** 1
[153] Goering E, Schramme M, Müller O, Paulin H, Klemm M, den Boer M L and Horn S 1997 *Physica* B **230–232** 996
[154] Guo Q L and Møller P J 1995 *Surf. Sci.* **340** L999
[155] Condon N G, Leibsle F M, Lennie A R, Murray P W, Parker T M, Vaughan D J and Thornton G 1998 *Surf. Sci.* **397** 278
[156] Weiss W and Ritter M 1999 *Phys. Rev.* B **59** 5201
[157] Yi S I, Liang Y, Thevuthasan S and Chambers S A 1999 *Surf. Sci.* **443** 212
[158] Chambers S A and Yi S I 1999 *Surf. Sci.* **439** L785
[159] Yi S I, Liang Y and Chambers S A 1999 *J. Vac. Sci. Technol.* A **17** 1737
[160] Guiot E, Wu Z Y, Gota S and Gautier-Soyer M 1999 *J. Electron Spectrosc. Relat. Phenom.* **101–103** 371
[161] Fujii T, Alders D, Voogt F C, Hibma T, Thole B T and Sawatzky G A 1996 *Surf. Sci.* **366** 579
[162] Lad R J and Henrich V E 1988 *Surf. Sci.* **193** 81
[163] Shaikhutdinov Sh K and Weiss W 1999 *Surf. Sci. Lett.* **432** L627
[164] Wang X G, Weiss W, Shaikhutdinov S K, Ritter M, Petersen M, Wagner F, Schlögl R and Scheffler M 1998 *Phys. Rev. Lett.* **81** 1038
[165] Wasserman E, Rustad J R, Felmy A R, Hay B P and Halley J W 1997 *Surf. Sci.* **385** 217
[166] Thevuthasan S, Kim Y J, Yi S I, Chambers S A, Morais J, Denecke R, Fadley C S, Liu P, Kendelewicz T and Brown G E 1999 *Surf. Sci.* **425** 276
[167] Chung M F and Farnsworth H E 1970 *Surf. Sci.* **22** 93
[168] Levine J D, Willis A, Bottoms W R and Mark P 1972 *Surf. Sci.* **29** 144
[169] Fiermans L, Arijs E, Vennik J and Maenhout-van der Vorst W 1973 *Surf. Sci.* **39** 357
[170] van Hove H and Leysen R 1972 *Phys. Status Solidi* a **9** 361
[171] Leysen R, van Orshaegen G, van Hove H and Neyens A 1973 *Phys. Status Solidi* a **18** 613
[172] Chang S C and Mark P 1974 *Surf. Sci.* **46** 293
[173] Henrich V E, Zeiger H J, Solomon E I and Gay R R 1978 *Surf. Sci.* **74** 682
[174] Overbury S H, Radulovic P V, Thevuthasan S, Herman G S, Henderson M A and Peden C H F 1998 *Surf. Sci.* **410** 106
[175] Rohrer G S and Bonnell D A 1991 *Surf. Sci.* **247** L195
[176] Parker T M, Condon N G, Lindsay R, Leibsle F M and Thornton G 1998 *Surf. Sci.* **415** L1046
[177] Duke C B and Lubinsky A R 1975 *Surf. Sci.* **50** 605
[178] Sambi M, Granozzi G, Rizzi G A, Casarin M and Tondello E 1994 *Surf. Sci.* **319** 149
[179] Galeotti M, Atrei A, Bardi U, Rovida G, Torrini M, Zanazzi E, Santucci A and Klimov A 1994 *Chem. Phys. Lett.* **222** 349
[180] Jedrecy N, Sauvage-Simkin M and Pinchaux R 2000 at press
[181] Jacobi K, Zwicker G and Gutmann A 1984 *Surf. Sci.* **141** 109
[182] Göpel W, Pollmann J, Ivanov I and Reihl B 1982 *Phys. Rev.* B **26** 3144
[183] Girard R T, Tjernberg O, Chiaia G, Söderholm S, Karlsson U O, Wigren C, Nylen H and Lindau I 1997 *Surf. Sci.* **373** 409
[184] Møller P J, Komolov S A and Lazneva E F 1999 *J. Phys.: Condens. Matter* **11** 9581
[185] Tsukada M, Miyazaki E and Adachi H 1981 *J. Phys. Soc. Japan* **50** 3032
[186] Kuwabara R, Adachi H and Morimoto T 1988 *Surf. Sci.* **193** 271
[187] Martins J B L, Longo E and Andres J 1993 *Int. J. Quantum Chem.: Quantum Chem. Symp.* **27** 643
[188] Gibson A, unpublished
[189] Noguera C 2000 to be published
[190] Goniakowski J and Noguera C 1996 *Surf. Sci.* **365** L657
[191] Powell R A and Spicer W E 1976 *Phys. Rev.* B **13** 2601
[192] Henrich V E, Dresselhaus G and Zeiger H J 1978 *Phys. Rev.* B **17** 4908
[193] Courths R, Cord B and Saalfeld H 1989 *Solid State Commun.* **70** 1047

[194] Cord B and Courths R 1985 *Surf. Sci.* **162** 34
[195] Tanaka Y, Morishita H, Watamori M, Oura K and Katayama I 1994 *Appl. Surf. Sci.* **82–83** 528
[196] Liang Y and Bonnell D A 1994 *Surf. Sci.* **310** 128
[197] Bickel N, Schmidt G, Heinz K and Muller K 1989 *Phys. Rev. Lett.* **62** 2009
[198] Hikita T, Hanada T, Kudo M and Kawai M 1993 *J. Vac. Sci. Technol.* A **11** 2649
[199] Hikita T, Hanada T, Kudo M and Kawai M 1993 *Surf. Sci.* **287–288** 377
[200] Mackrodt W C 1988 *Phys. Chem. Minerals* **15** 228
[201] Prade J, Schroder U, Kress W, de-Wette F W and Kulkarni A D 1993 *J. Phys.: Condens. Matter* **5** 1
[202] Padilla J and Vanderbilt D 1998 *Surf. Sci.* **418** 64
[203] Li Z Q, Zhu J L, Wu C Q, Tang Z and Kawazoe Y 1998 *Phys. Rev.* B **58** 8075
[204] Wolfram T, Hurst R and Morin F J 1973 *Phys. Rev.* B **7** 1677
[205] Wolfram T, Hurst R and Morin F J 1977 *Phys. Rev.* B **15** 1151
[206] Tsukada M, Satoko C and Adachi H 1980 *J. Phys. Soc. Japan* **48** 200
[207] Kimura S, Yamauchi J, Tsukada M and Watanabe S 1995 *Phys. Rev.* B **51** 11 049
[208] Liang Y, Rothman J B and Bonnell D A 1994 *J. Vac. Sci. Technol.* A **12** 2276
[209] Liang Y and Bonnell D A 1995 *J. Am. Ceram. Soc.* **78** 2633
[210] Liang Y and Bonnell D A 1993 *Surf. Sci.* **285** L510
[211] Matsumoto T, Tanaka H, Kawai T and Kawai S 1992 *Surf. Sci.* **278** L153
[212] Tanaka H, Matsumoto T, Kawai T and Kawai S 1993 *Japan. J. Appl. Phys.* I **32** 1405
[213] Tanaka H, Matsumoto T, Kawai T and Kawai S 1994 *Surf. Sci.* **318** 29
[214] Matsumoto T, Tanaka H, Kouguchi K, Kawai T and Kawai S 1994 *Surf. Sci.* **312** 21
[215] Kubo A, Tanaka H, Tabata H, Matsumoto T and Kawai T 1996 *Japan. J. Appl. Phys.* II **35** L1692
[216] Andersen J E T and Møller P J 1990 *Appl. Phys. Lett.* **56** 1847
[217] Kimura S and Tsukada M 1997 *Appl. Surf. Sci.* **121–122** 195
[218] Ferrer S and Somorjai G A 1980 *Surf. Sci.* **94** 41
[219] Tanaka H and Kawai T 1996 *Surf. Sci.* **365** 437
[220] Sigmund W M, Rotov M, Jiang Q D, Brunen J, Zegenhagen J and Aldinger F 1997 *Appl. Phys.* A **64** 219
[221] Sekiguchi S, Fujimoto M, Kang M-G, Koizumi S, Cho S-B and Tanaka J 1998 *Japan. J. Appl. Phys.* **37** 4140
[222] Aiura Y, Bando H, Nishihara Y, Haruyama Y, Kodaira S, Komeda T, Sakisaka Y, Maruyama T and Kato H 1994 *Advances in Superconductivity VI* (Tokyo: Springer)
[223] Bando H, Aiura Y, Haruyama Y, Shimizu T and Nishihara Y 1995 *J. Vac. Sci. Technol.* B **13** 1150
[224] Brunen J and Zegenhagen J 1997 *Surf. Sci.* **389** 349
[225] Hagendorf C, Schindler K M, Doege T and Neddermeyer H 1998 *Surf. Sci.* **402** 581
[226] Pojani A, Finocchi F and Noguera C 1999 *Appl. Surf. Sci.* **142** 177
[227] Pojani A, Finocchi F and Noguera C 1999 *Surf. Sci.* **442** 179
[228] Farrell H H, Harbison J P and Peterson L D 1987 *J. Vac. Sci. Technol.* B **5** 1482
[229] Pashley M D 1989 *Phys. Rev.* B **40** 10 481
[230] Harrison W A 1979 *J. Vac. Sci. Technol.* **16** 1492
[231] LaFemina J P 1996 *Handbook of Surface Science I* ed W N Unertl (Amsterdam: Elsevier) ch 4, p 137
[232] Godin T J and LaFemina J P 1994 *Phys. Rev.* B **49** 7691
[233] Noguera C, Pojani A and Finocchi F 2000 submitted
[234] Harrison W A 1980 *Electronic Structure and the Properties of Solids* (San Francisco, CA: Freeman)
[235] Albaret T, Finocchi F and Noguera C 1999 *Discuss. Faraday Soc.* **114** 285
[236] Goniakowski J and Noguera C 1994 *Surf. Sci.* **319** 68
[237] Goniakowski J and Noguera C 1994 *Surf. Sci.* **319** 81
[238] Goniakowski J and Noguera C 1995 *Surf. Sci.* **323** 129
[239] Oliver P M, Parker S C and Mackrodt W C 1993 *Modell. Simul. Mater. Sci. Eng.* **1** 755
[240] Noguera C 1996 *J. Adhes.* **57** 91
[241] Finocchi F and Noguera C 2000 *J. Adhes.* at press